AD-A133 883 LONG TERM UPPER OCEAN STUDY (LOTUS) AT 34 DEG N 70 DEG W: METEOROLOGICAL. (U) WOODS HOLE OCEANOGRAPHIC INSTITUTION MA C DESER ET AL. SEP 83 WHOI-83-32 1/1

UNCLASSIFIED N00014-76-C-0197 F/G 4/2 NL

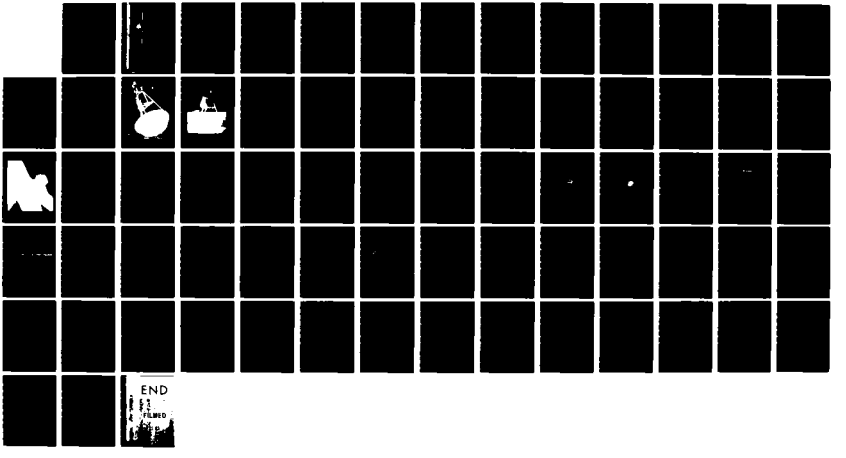

END

FILMED

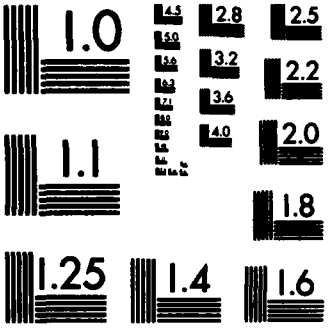

MICROCOPY RESOLUTION TEST CHART
NATIONAL BUREAU OF STANDARDS-1963-A

WHOI-83-32

Woods Hole Oceanographic Institution

Long Term Upper Ocean Study (LOTUS) at 34°N, 70°W: Meteorological Sensors, Data, and Heat Fluxes for May-October 1982 (LOTUS-3 and LOTUS-4)

by

Clara Deser, Robert A. Weller
and
Melbourne G. Briscoe

September 1983

Technical Report

Prepared for the Office of Naval Research under Contract N00014-76-C-0197; NR 083-400.

Approved for public release; distribution unlimited.

WOODS HOLE, MASSACHUSETTS 02543

50272-101

REPORT DOCUMENTATION PAGE	1. REPORT NO. WHOI-83-32	2.	3. Recipient's Accession No. AD-A133 883
4. Title and Subtitle: Long Term Upper Ocean Study (LOTUS) at 34°N, 70°W: Meteorological Sensors, Data, and Heat Fluxes for May-October 1982 (LOTUS-3 and LOTUS-4)			5. Report Date: September 1983 6.
7. Author(s): Clara Deser, Robert A. Weller and Melbourne G. Briscoe			8. Performing Organization Rept. No. WHOI-83-32
9. Performing Organization Name and Address: Woods Hole Oceanographic Institution, Woods Hole, Massachusetts 02543			10. Project/Task/Work Unit No. 11. Contract(C) or Grant(G) No. (C) N00014-76-C-0197; (G) NR 083-400
12. Sponsoring Organization Name and Address: Office of Naval Research, Environmental Sciences Directorate, Arlington, VA 22217			13. Type of Report & Period Covered: Technical 14.

15. Supplementary Notes: This report should be cited as: Woods Hole Oceanog. Inst. Tech. Rept. WHOI-83-32.

16. Abstract (Limit: 200 words)

Meteorological data have been gathered from a moored surface buoy at 34°N, 70°W in the Long Term Upper Ocean Study (LOTUS) experiment. The meteorological results from the first year of LOTUS are encouraging; the data returned from redundant sensors agree closely. Surface heat fluxes calculated from the observations show the annual cycle of heat transfer to the mixed layer.

This report documents the meteorological sensors on the LOTUS-3 (May 1982-October 1982) and LOTUS-4 (November 1982-March 1983) surface buoys. It describes in detail the telemetry of the meteorological data via the ARGOS satellite system. The measurements returned from LOTUS-3 are presented and evaluated. Monthly heat fluxes at the sea surface are computed using the bulk formulas and compared with the long-term means. The errors in the heat fluxes have been estimated.

17. Document Analysis a. Descriptors

1. Heat flux
2. Air-Sea Interaction
3. Buoy

b. Identifiers/Open-Ended Terms

c. COSATI Field/Group

18. Availability Statement: Approved for public release; distribution unlimited.	19. Security Class (This Report): Unclassified	21. No. of Pages: 68
	20. Security Class (This Page)	22. Price

(See ANSI-Z39.18) See Instructions on Reverse OPTIONAL FORM 272 (4-77) (Formerly NTIS-35) Department of Commerce

WHOI-83-32

Long Term Upper Ocean Study (LOTUS) at 34°N, 70°W: Meteorological Sensors, Data, and Heat Fluxes for May-October 1982 (LOTUS-3 and LOTUS-4)

by

Clara Deser, Robert A. Weller
and
Melbourne G. Briscoe

Woods Hole Oceanographic Institution
Woods Hole, Massachusetts 02543

September 1983

Technical Report

Prepared for the Office of Naval Research under Contract N00014-76-C-0197; NR 083-400.

Approved for Distribution:

N. P. Fofonoff

N. P. Fofonoff, Chairman
Department of Physical Oceanography

Abstract

Meteorological data have been gathered from a moored surface buoy at 34°N, 70°W in the Long Term Upper Ocean Study (LOTUS) experiment. The meteorological results from the first year of LOTUS are encouraging; the data returned from redundant sensors agree closely. Surface heat fluxes calculated from the observations show the annual cycle of heat transfer to the mixed layer.

This report documents the meteorological sensors on the LOTUS-3 (May 1982-October 1982) and LOTUS-4 (November 1982-March 1983) surface buoys. It describes in detail the telemetry of the meteorological data via the ARGOS satellite system. The measurements returned from LOTUS-3 are presented and evaluated. Monthly heat fluxes at the sea surface are computed using the bulk formulas and compared with the long-term means. The errors in the heat fluxes have been estimated.

TABLE OF CONTENTS

LIST OF FIGURES

LIST OF TABLES

I. INTRODUCTION

The Long Term Upper Ocean Study (LOTUS) is a two year experiment (May 1982-May 1984) designed to collect meteorological and oceanographic data within a two-degree square in the Sargasso Sea. The data will be used to examine the low frequency variability (days to months) in the internal wave field and the energy budget of the mixed layer. (For an introduction to the experiment, see Trask, Briscoe and Pennington, 1982.) Meteorological data are gathered from a moored surface buoy. The surface mooring set 12 May 1982 and retrieved 30 October 1982 is referred to as LOTUS-3; the surface mooring set 31 October 1982 and retrieved 10 March 1983 as LOTUS-4. The LOTUS-3 and LOTUS-4 surface buoys were equipped with three sets of meteorological sensors. The parameters measured from each buoy included air temperature, sea temperature, wind speed and direction, solar radiation and barometric pressure. (Relative humidity was also measured from LOTUS-4.) Duplication of each type of sensor provided redundancy in case of failure and the opportunity for comparisons between instruments. The data from two sets of sensors were auto-recorded by two Vector-Averaging Wind Recorders. The data from the third set of sensors were telemetered via the ARGOS Satellite System. This report describes the meteorological sensors (primarily the telemetering sensors) on the LOTUS-3 and LOTUS-4 surface buoys, and presents the data returned (primarily from LOTUS-3). One purpose of the meteorological measurements is to compute the heat fluxes at the sea surface using the bulk aerodynamic formulas (Large and Pond, 1982; and Bunker, 1975, 1976). This report outlines the bulk formulas and presents estimates of the monthly heat fluxes during May 1982-March 1983. We used comparisons between redundant sensors to determine the errors in the measurements; this gave a realistic estimate of the expected errors in our heat fluxes.

II. THE SURFACE BUOY

The LOTUS area is centered at 34°N, 70°W, 600 km east of Cape Hatteras, North Carolina, and 300 km south of the mean axis of the Gulf Stream (Figure 1). The LOTUS surface buoy is moored in approximately 5400 m of water. The buoy is recovered and replaced every six months for the duration of the experiment; the deployment schedule of LOTUS surface buoys is listed in Table 1.

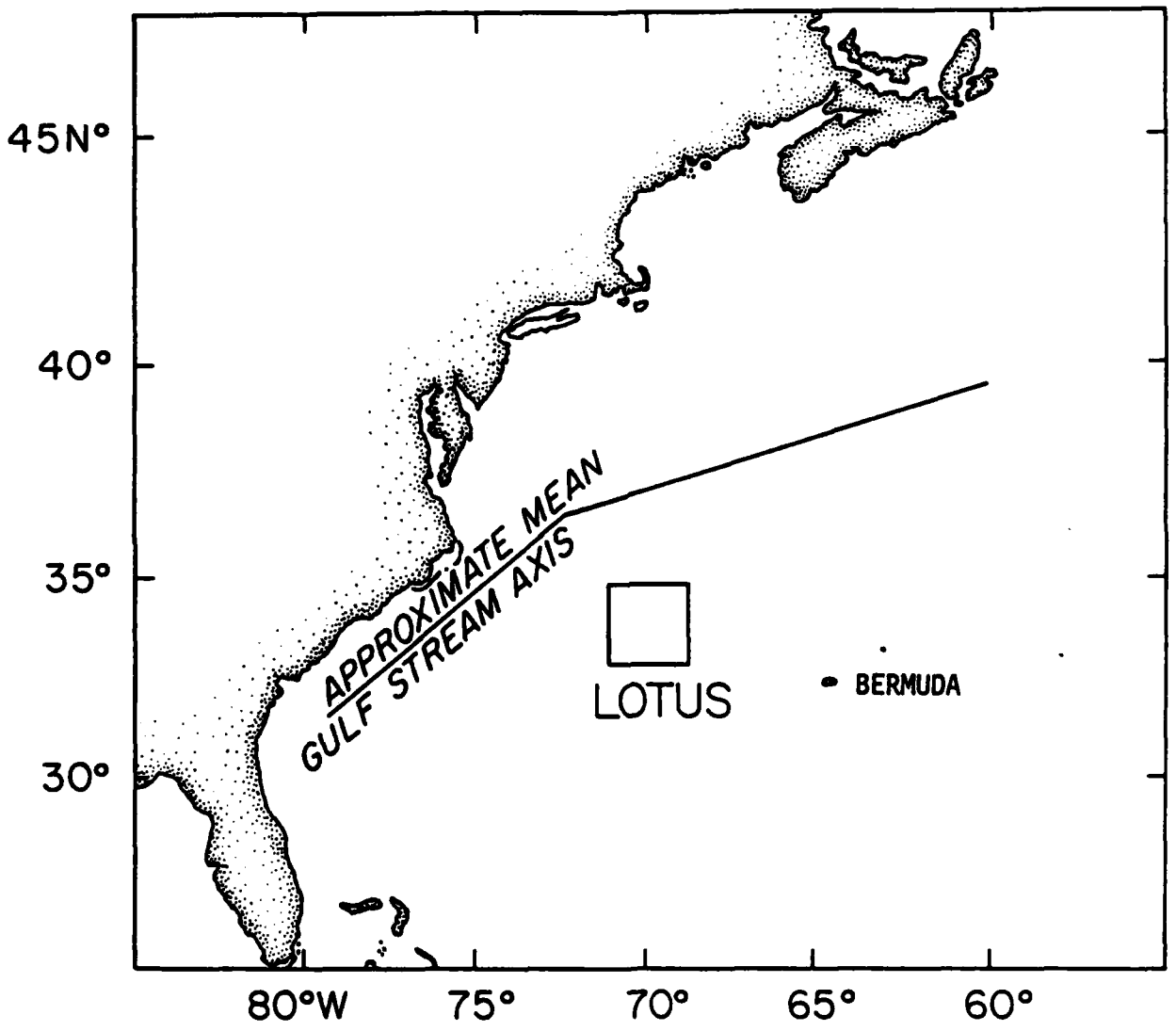

Figure 1. The ocatior _ the Long Term Upper Ocean Study area.

TABLE 1

EVENT	DATE
Cruise - OCEANUS 119	May 6-14, 1982
Surface Mooring - LOTUS-3	May 12-October 30, 1982
Cruise - OCEANUS 129	October 28-November 4, 1982
Surface Mooring - LOTUS-4	October 31, 1982-March 9, 1983
Cruise - ENDEAVOR 97	April 8-19, 1983
Surface Mooring - LOTUS-5	April 12-October 1983*
Cruise - OCEANUS*	October 1983*
Surface Mooring - LOTUS-6	October 1983*-May 1984*
Cruise - OCEANUS*	May 1984*

* planned

The LOTUS surface buoy, shown in Fig. 2, is a 10' (3.05 m) diameter WHOI discus buoy designed by H. O. Berteaux at the Woods Hole Oceanographic Institution. The buoy hull and removable tower are constructed of 6061 aluminum alloy. The watertight hull is divided into three chambers and a central instrument well. The entire hull, except for the instrument well, is filled with low density rigid foam to prevent flooding. The foam is polyurethane H-102-N (density = 2 lbs ft^{-3} = 6.5 g m^{-3}), manufactured by Allied Resins Corporation. The buoy hull weighs 1650 lbs (750 kg) without foam, 1970 lbs (895 kg) with foam, and has a maximum buoyancy of 9550 lbs (4336 kg). Although subject to strong heave and roll motion under low tension conditions, the discus buoy provides ample buoyancy to offset the normally high mooring line tension and contributes little drag to the mooring system. The steel rigid bridle increases the righting moment of the buoy by lowering the point of attachment of the mooring line. According to our observations, the buoy stays within 10° of vertical, even in 3 m seas.

The instrument well on the LOTUS-3 and LOTUS-4 buoys contains a battery for the navigation light, a battery for the meteorological sensors, an ARGOS satellite transmitter terminal and battery, and an electrical switch to detect water in the well. In addition, the instrument well on the LOTUS-4 buoy houses the electronics and recording packages of both Vector Averaging Wind Recorders (VAWRs) and the VAWR battery packs (Figure 3).

The removable tower serves as a platform for the meteorological sensors, the navigation light, and the satellite antenna. The orienting vane on the buoy keeps the three wind sensors on the upwind side of the tower.

III. METEOROLOGICAL SENSORS

Figures 4 and 5 show the configuration of the meteorological sensors on the LOTUS-3 and 4 buoy towers, respectively. For reference, a summary of the meteorological sensors and sensor specifications is compiled in Table 2. The mean height of each sensor above the water is listed in Table 3.

The buoy is a difficult platform from which to make accurate meteorological measurements. On the buoy, the sensors are subjected to pitch and roll and contamination by salt spray. Nearby sensors and the buoy tower can obstruct the wind flow to the sensors. These severe conditions can degrade

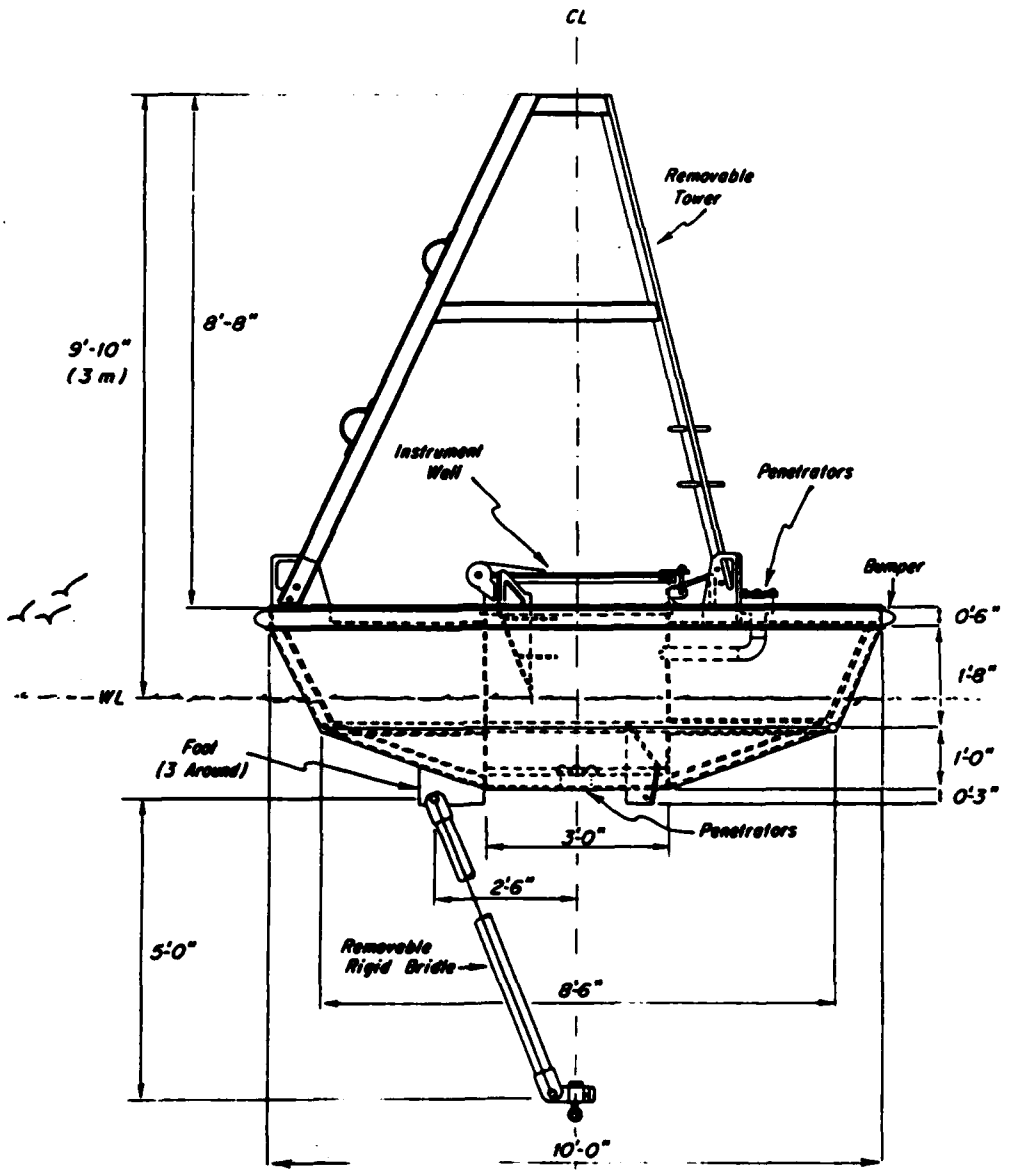

10 FT. WHOI DISCUS BUOY

Figure 2. Diagram of the LOTUS surface buoy.

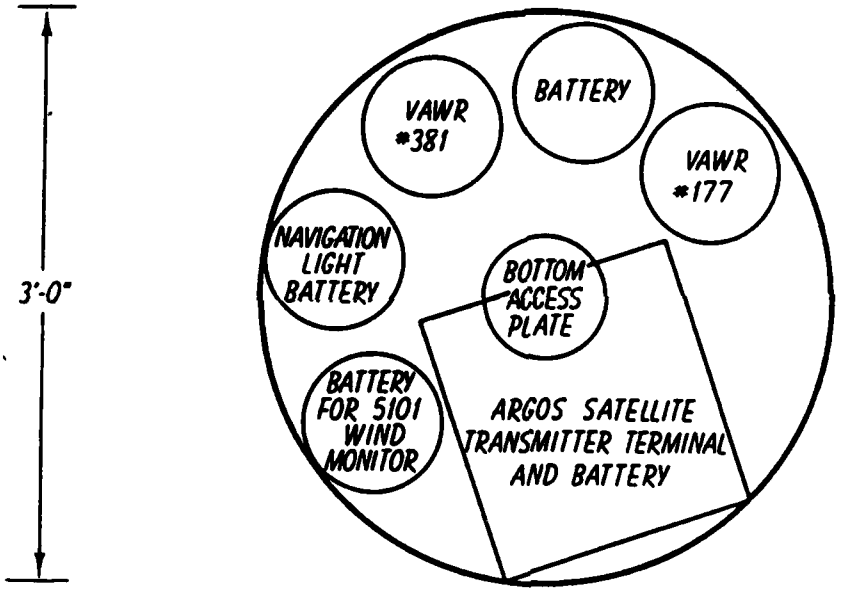

LOTUS IV INSTRUMENT WELL LAYOUT

Figure 3. Contents of the instrument well on LOTUS-4.

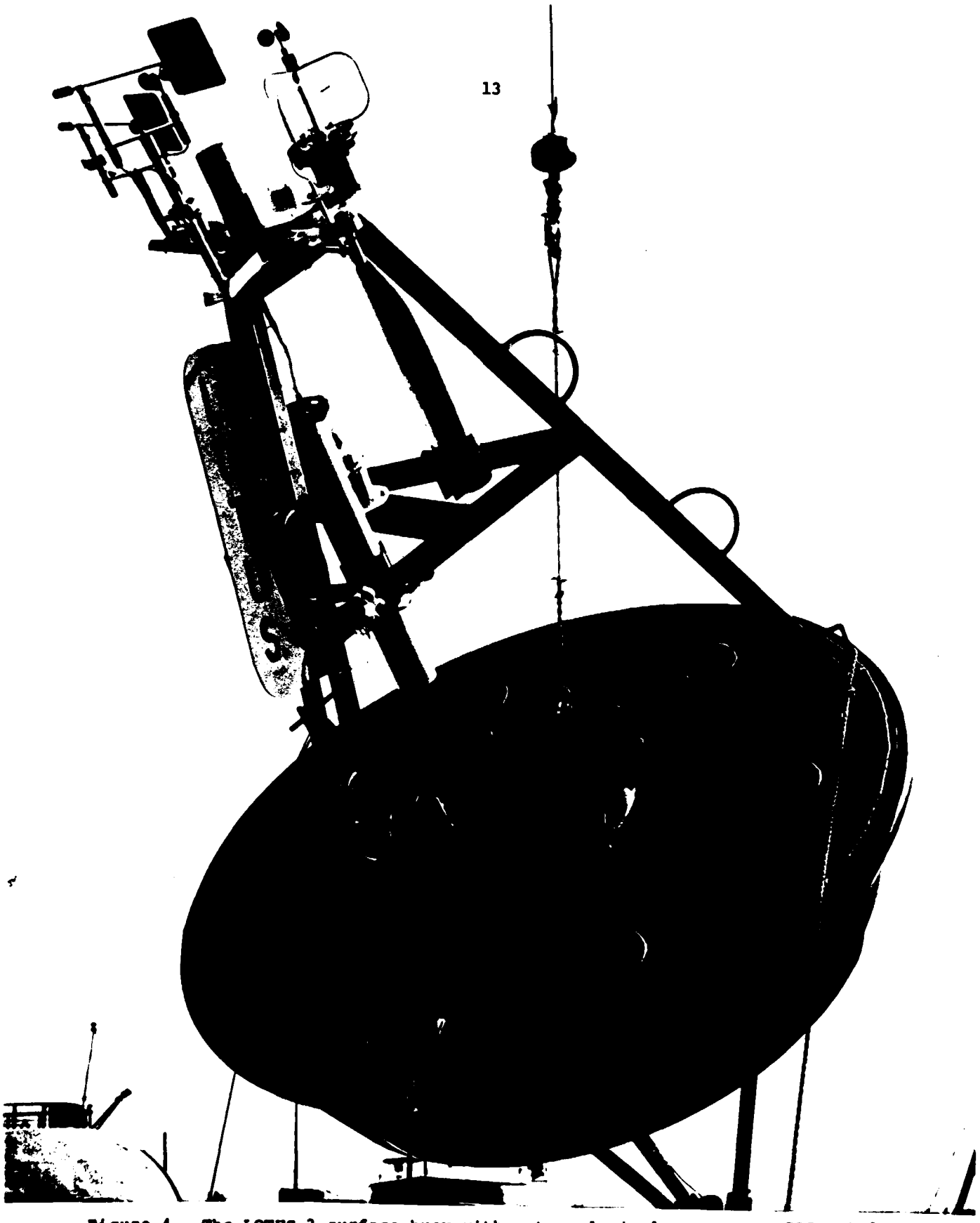

Figure 4. The LOTUS-3 surface buoy with meteorological sensors, ARGOS satellite antenna, and navigation light. The orienting vane keeps the three wind sensors on the upwind side of the tower.

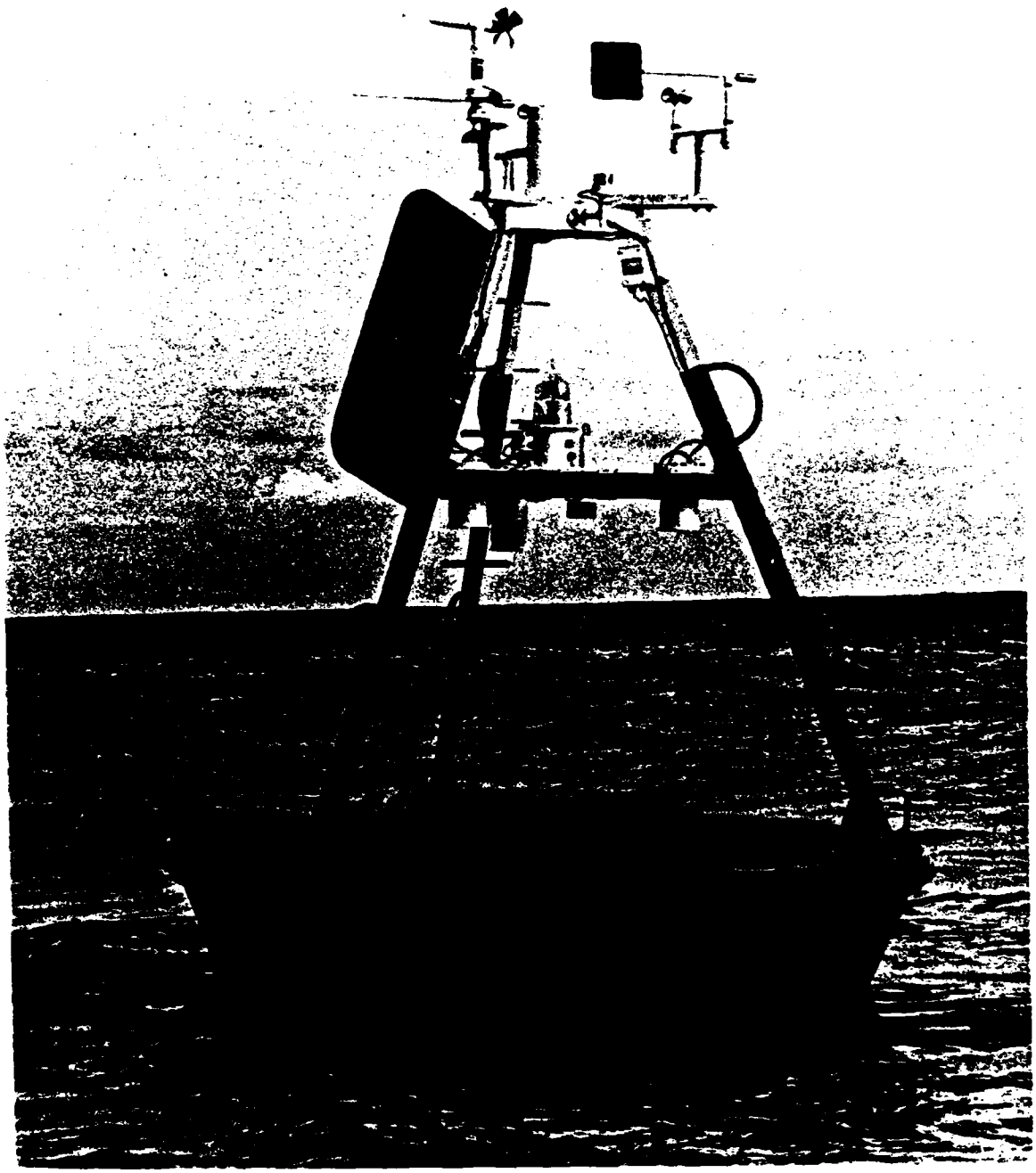

Figure 5. The LOTUS-4 surface buoy with meteorological sensors, ARGOS satellite antenna, and navigation light. The orienting vane keeps the three wind sensors on the upwind side of the tower.

TABLE 2

TABLE 2: METEOROLOGICAL SENSORS

	Parameter	Sensor	Manufacturer	Range	Sensor Accuracy	System Accuracy	LOTUS-3	LOTUS-4	Comments
TELEMETERED	1. Wind speed	Gill 3-cup anemometer	R.M. Young Co., model 6301	0-54 m/s	See Text	0.2 m/s(r)	X	X	
	2. Wind direction	Vane	R.M. Young Co., model 6101	0-360°	See Text	5°(s)	X	X	
	3. Air temperature	Thermistor with Thaller Shield	Yellow Springs Instrument Co., model 44034	±35°C	0.1°C	0.5°C(s)	X	X	
	4. Hull temperature	Thermistor	Yellow Springs Instrument Co., Model 44034	±30°C	0.1°C	0.3°C(s)	X	X	
	5. Barometric pressure	Digiquartz with Gill Pressure port	Paroscientific, Inc. Model 215	0-1034 mb	0.2 mb	0.5 mb(m)	X		
		Aneroid	Yellow Springs Instrument Co., model 2014-28/35 HA-3-MB	984-1084 mb	3 mb	5 mb(r)		X	
	6. Tension (at top of moorings)	Hydraulic piston	W. Swift Co., Bourne, MA	0-9300 lbs.		40 lbs(r)	X	X	
VAMR 1	1. Wind speed	Gill 3-cup anemometer	R.M. Young Co., model 6301	0-54 m/s	See Text	0.1 m/s(r)	X	X	LOTUS-3, #184, Sampling rate: 3.75 min
	2. Wind direction	Vane	R.M. Young Co., model 6101	0-360°	See Text	5°(s)	X	X	LOTUS-4, #177, Sampling rate: 7.5 min.
	3. Air temperature	Thermistor with Thaller Shield	Yellow Springs Instrument Co., model 44034	±35°C	0.1°C	0.3°C(m)	X	X	
	4. Sea temperature	Thermistor	Thermometrics Co.	±30°C	0.004°C	0.01°C(e)	X	X	
	5. Solar radiation	Pyranometer	Eppley Co., model 8-48	0-1400W/m^2	3%	5%(m)		X	
			NYCAL Eng., model P-6405-A	0-1400W/m^2	3%	5%(m)	X		
	6. Relative humidity	Strain gauge	NYCAL Eng., model HS-3552-B	0-100%	6%	(*)		X	(*) failed after one month
VAMR 2	1. Wind speed and direction	Integral 3-cup anemometer and vane	WHOI	0-54 m/s 0-360°	See Text	0.1 m/s(s)	X		LOTUS-3, #537, Sampling rate: 3.75 min
	2. Wind Speed and direction	Propeller and vane	R.M. Young Co., model 5101	0-50 m/s 0-360°	See Text	5°(s)		X	LOTUS-4, #381, Sampling rate: 7.5 min.
	3. Air temperature	Thermistor with PML shield	Yellow Springs Instrument Co., model 44034 housing - Polar Research Labs.	±35°C	0.1°C	2°C(s)	X		
	4. Barometric pressure	Digiquartz with Gill Pressure port	Paroscientific, Model 215-AS-002	0-1034 mb	0.1 mb	0.5 mb(m)	X	X	
	5. VAMR electronic chassis temperature	Thermistor	Yellow Springs Instrument Co., Model 44034	±35°C	0.1°C	0.1°C(e)		X	Engineering test sensor

(r) ARGOS digitization resolution
(s) Scatterplot estimate
(m) Manufacturer's value
(e) Estimate based on previous experience

TABLE 3

Nominal height above water line (meters)

Telemetered Sensors	LOTUS-3	LOTUS-4
1. Wind (Gill 3-cup anemometer and vane)	3.6	3.6
2. Air thermistor with Thaller Shield	2.9	3.1
3. Barometer (Digiquartz LOTUS-3, Aneroid LOTUS-4)	2.0	2.6
4. Sea thermistor	-0.6	-0.6
5. Compass	2.0	2.0

VAWR Sensors	#184	#177
1. Pyranometer (Insolation)	2.9	3.2
2. Wind (Gill 3-cup anemometer and vane)	3.3	3.6
3. Air thermistor (with Thaller Shield)	2.9	3.1
4. Sea thermistor	-0.6	-0.6
5. Relative humidity	--	1.8
6. Compass	2.0	2.0

VAWR Sensors	#537	#381
1. Wind (Integral LOTUS-3, 5101 LOTUS-4)	3.2 vane/3.6 cups	3.8
2. Air thermistor	2.9	3.0
3. Barometer (Digiquartz)	3.0	2.6
4. Compass	2.0	2.0

the accuracy of the measurements. We have taken some general precautions to overcome the hazards of the buoy's environment:

1) The rigid bridle and taut-mooring line reduce the tilt of the buoy to within 10° of vertical,
2) The orienting vane on the buoy tower keeps the sensors upwind,
3) Many of the sensors have shields to protect from them direct sunlight and spray.

Vector-Averaging Wind Recorder

The Vector-Averaging Wind Recorder (VAWR), an adaptation of the Vector Averaging Current Meter (VACM), was designed at WHOI for making high quality, long duration observations of meteorological parameters from moored oceanic buoys. The VAWR contains integrating and recording circuitry which computes vector-averaged wind velocity. The VAWR also provides several channels for recording additional measurements. In its original deployment during the 1972 Joint Air-Sea Interaction (JASIN) experiment, the VAWR measured incident solar radiation, wind speed and direction, air temperature, sea surface temperature, relative humidity and barometric pressure (Payne, 1974). The VAWRs used in LOTUS were fitted with more responsive wind sensors and were designed to cause much less flow disturbance around the wind sensors than the VAWR used previously. Two VAWRs were mounted on the tower of LOTUS-3. On LOTUS-4, the VAWR electronics packages were placed inside the instrument well primarily to increase the mechanical stability of the buoy, to prevent theft by vandals of the self-recorded data, and to more fully expose the navigation light on the tower. The VAWRs on LOTUS-3, serial No. 184 and No. 537, recorded data averaged over 3.75 min; those on LOTUS-4, serial No. 177 and No. 381, recorded data averaged over 7.5 min. The averaging interval was thus doubled to accommodate the extra relative humidity data being recorded on LOTUS-4. These sampling rates were long enough to average out the bulk of the buoy motion effects but still short enough to retain high-frequency variability in the meteorological data.

Wind Velocity

1) Gill Wind Vane and Cup Anemometer

The Gill Wind Vane and Cup Anemometer (model 6101/6301) is a utility wind instrument designed by Professor G. Gill at the University of Michigan, and manufactured by R. M. Young Company. A sketch of this set is shown in

Fig. 6. The cup assembly is mounted on a stainless steel shaft which rotates and drives a d.c. tachometer generator located in the lower housing. A fixed Sony magnetodiode counts the rotations of the anemometer cups by sensing a magnet mounted on the rotor shaft. An analog voltage derived from the diode counts is directly proportional to wind speed throughout the working range (see calibration curve in Fig. 7). The aluminum cups have a turning radius of 4.4 cm and a threshold less than 0.7 m s^{-1}. The cup assembly has a distance constant* of 3.7 m (Payne, 1981). The cup anemometer is relatively insensitive to tilt; for tilts less than 20°, the maximum expected from a taut-moored discus buoy, the anemometer response was within 5 percent of the response when vertical (Payne, 1981). The wind vane (model 6301) is made of sheet aluminum and has a threshold less than 0.7 m s^{-1}. The vane utilizes a 10^3 ohm conductive-plastic potentiometer mounted in the lower part of the main housing to generate an analog voltage output signal which is directly proportional to wind direction relative to buoy orientation. The sum of the orientations of the Gill Vane and the buoy is the direction of the wind relative to magnetic north. The Gill Vane has a response distance of 1.4 m and a damping ratio of 0.37 (Payne, 1981). Under wind tunnel conditions, the linearity of the wind anemometer is 1 percent (manufacturer's value).

Two Gill wind sensors were used on both LOTUS-3 and LOTUS-4; the data from one sensor were telemetered, and from the other recorded on VAWR No. 184, LOTUS-3 and No. 177, LOTUS-4.

2) Integral Cup and Vane

This instrument, designed by J. Dean (WHOI), uses cups from the Gill Wind Vane and Cup Anemometer (R. M. Young model 6101/6301) (see Fig. 6). Three

---

*The dynamic response of a wind speed/direction sensor can be summarized by three quantities: the distance constant of the anemometer, the delay distance of the vane, and the damping ratio of the vane. The distance constant is a measure of the response of a rotating wind sensor to a change in wind velocity. It is the displacement of air past the sensor during the time required for the anemometer to adjust to the new wind speed. The delay distance is the displacement of air past the wind vane during the time it takes for the vane to adjust to the new wind direction. The damping ratio is the ratio of the actual to critical damping coefficients of the vane.

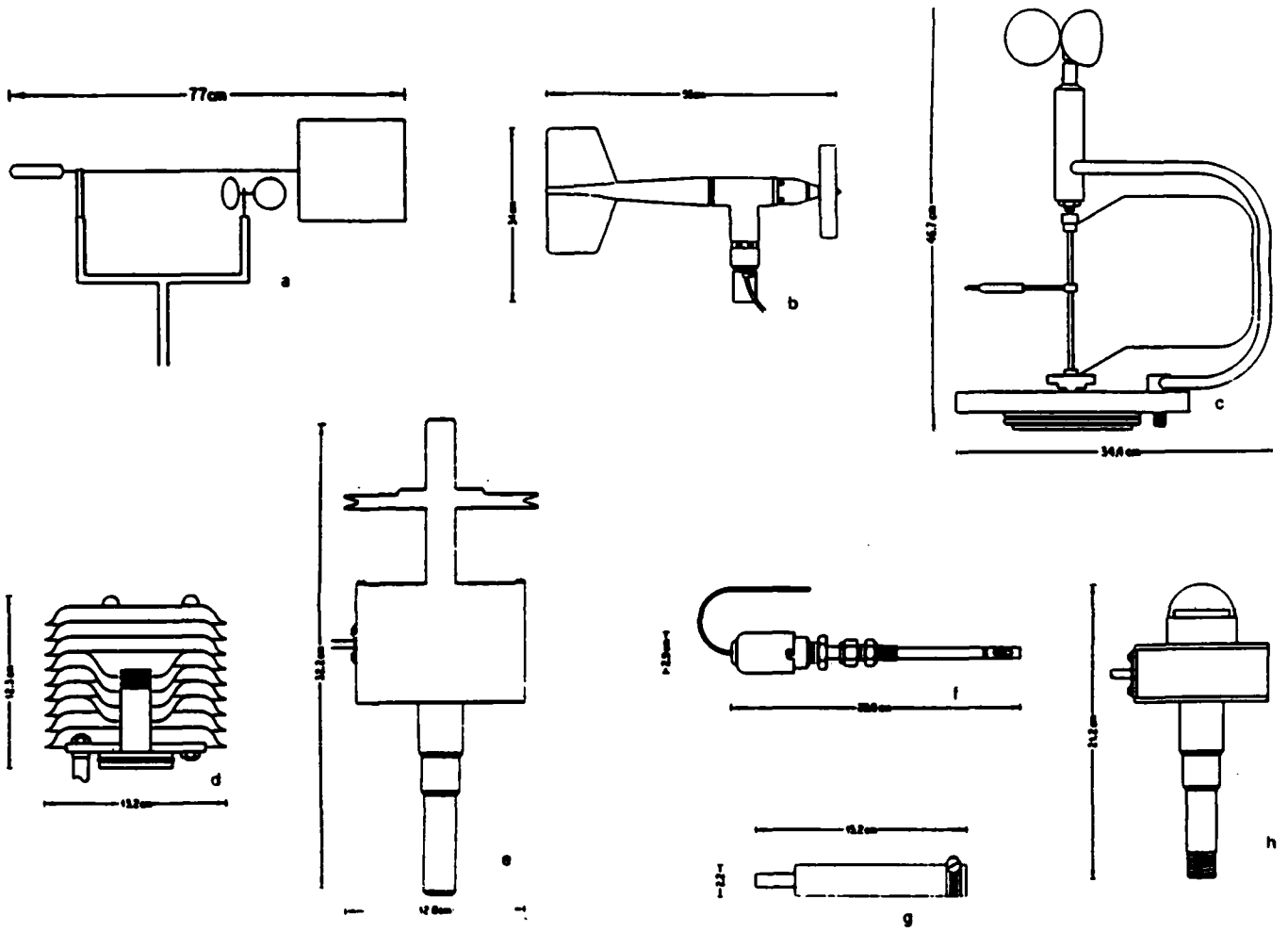

Figure 6. Schematic diagrams of the meteorological sensors on LOTUS-3 and LOTUS-4: (a) Gill 3-cup anemometer and vane, (b) Young 5101 Wind Monitor, (c) Integral 3-cup anemometer and vane, (d) Air temperature thermistor with Thaller shield, (e) Digiquartz barometric pressure case with pressure port (f) Hycal relative humidity sensor, (g) Sea temperature thermistor (h) Pyranometer.

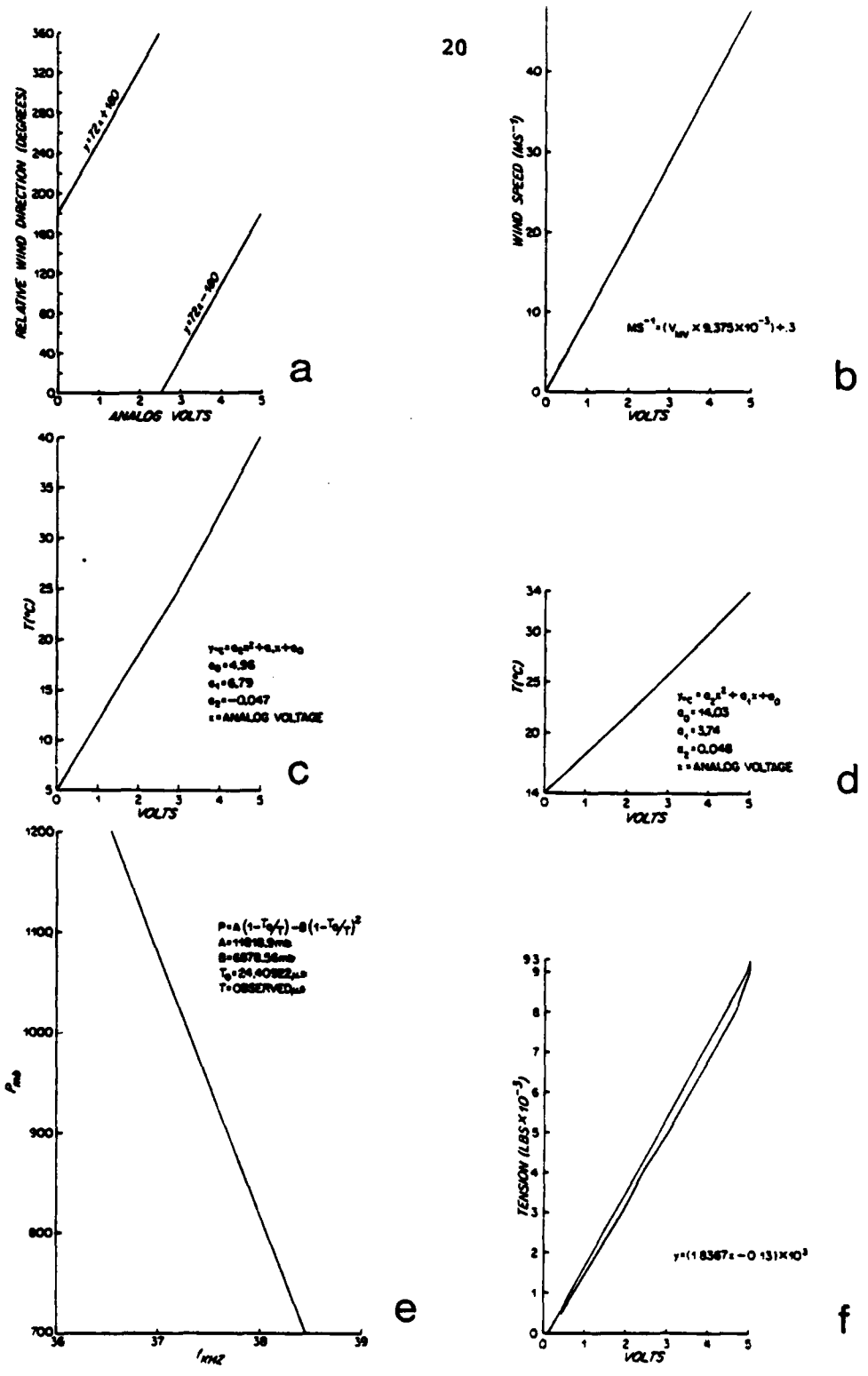

Figure 7. Calibration curves for the telemetered sensors: (a) Gill vane and (b) Anemometer, (c) Air temperature thermistor, (d) Hull temperature thermistor, (e) Digiquartz barometric pressure transducer, (f) Tensiometer (note hysteresis effect).

aluminum tubing arms support the cup assembly above the vane, and are oriented to allow minimum flow blockage to the vane. The vane is fabricated of G10 fiberglass sheet. The vane is magnetically coupled to the vane follower in the VAWR. The vane follower senses the attitude of the vane relative to the buoy. The advantage of "integrating" the vane with the VAWR is that the vane and the VAWR compass are aligned and fixed in the laboratory. This procedure lessens the possibility of misaligning the vane with respect to the VAWR compass. This instrument was used only on LOTUS-3; the data were recorded on VAWR No. 537.

3) Wind Monitor

The Wind Monitor (R. M. Young Company, model 5101) was developed specifically for ocean data-buoy use. The following information is taken from the R. M. Young catalogue of wind instruments. The 5101 wind speed sensor is a helicoid-shaped propeller molded of polypropylene plastic (Figure 6). The propeller has four blades of 18 cm length each. A magnetically-activated Hall effect sensor produces one voltage pulse per propeller revolution. The frequency of the pulses is directly proportional to wind speed (30 Hz = 8.9 m s^{-1}). The main housing and vane are thermoformed of rigid ultraviolet stabilized plastic. The vane position is normally transmitted through a flexible coupling to a potentiometer that produces an analog voltage output proportional to the azimuth of the vane. For LOTUS the system was modified by J. Dean to give digital output and not use the potentiometer.

The threshold for the propeller is 0.6 m s^{-1} and for the vane 1.0 m s^{-1}. The dynamic response of the wind monitor can be summarized by:

a) Distance constant of propeller, 3.3 m.

b) Delay distance of vane, 1.3 m.

c) Damping ratio of vane, 0.27.

The Wind Monitor was used only on LOTUS-4; the data were recorded on VAWR No. 381.

The wind sensors were mounted on the tower approximately 3.5 m above the water.

Air Temperature

1) Thermistor with Thaller radiation shield

The air temperature sensor was a glass bead thermistor manufactured by Yellow Springs Instrument Co. (YSI) (part No. 44034). To diminish the effects

of self-heating, a high resistance thermistor (5000 ohms at 25°C) was chosen. The calibration curve, shown in Figure 7, was derived as follows: the manufacturer's calibration curve related resistance to temperature, and resistance was converted to voltage through an operational amplifier. This gave a calibration curve relating measured voltage to temperature (i.e., resistance). The thermistor has an accuracy of 0.1°C over the range $\pm$ 35°C. The thermistor was sheltered by a Gill-modified Thaller shield (Gill, 1979) fabricated at WHOI. The WHOI-version shield consists of a stack of convex aluminum plates which protects the thermistor from direct sunlight while allowing circulation of air past it (Figure 6). This rugged durable shield stands up well to strong winds and salt spray. According to Gill (1979), the heating error of his Thaller shield at various sun elevations and wind speeds is less than 0.3°C. The time constant (time required for a 63 percent response following a step change in air temperature) is less than one minute. Air temperature fluctuates on a much slower time scale relative to this response time. Two air-temperature thermistors with Thaller shields were used on both LOTUS-3 and LOTUS-4. Data from one sensor were telemetered and data from the other sensor recorded on VAWR No. 184, LOTUS-3 and No. 177, LOTUS-4.

2) Thermistor with PRL radiation shield

The thermistor is YSI part No. 44034 as described above. The PolyVinyl-Chloride (PVC) housing, manufactured by Polar Research Laboratories (PRL), was designed as a radiation shield. We found that the PRL shield was affected by direct sunlight which caused it to overheat by as much as 2°C during the day (see Data Results). This sensor was used on LOTUS-3; the data were recorded on VAWR No. 537.

The air-temperature sensors were mounted on the tower at a height of approximately 3 m.

On LOTUS-4, a third thermistor was used for an engineering test and not intended as a redundant air-temperature sensor. The thermistor (YSI part No. 44034) was embedded in the VAWR electronics chassis. The data from this thermistor were recorded on VAWR No. 381.

Sea Temperature

The sea-temperature sensor used for telemetry was a high resistance thermistor (5000 ohms at 25°C) manufactured by Yellow Springs Instrument Co. (part

No. 44034). The thermistor has an accuracy of 0.1°C over the range ±30°C. The manufacturer supplied the calibration curve which relates resistance to temperature. Resistance was converted to voltage through an operational amplifier. The calibration curve shown in Figure 7, which relates temperature to voltage, fits the manufacturer's curve to better than 0.1°C. The thermistor was embedded in the aluminum bottom access plate of the buoy and actually measured the temperature of the underside of the buoy.

The second sea-temperature sensor used on LOTUS-3 and LOTUS-4 was a precision, high-resistance thermistor (4000 ohms at 25°C) manufactured by Thermometrics Company. The accuracy of this thermistor is 0.004°C; the system accuracy of this measurement is better than 0.01°C. Data from the Thermometrics thermistors were recorded on VAWR No. 184 (LOTUS-3) and No. 177 (LOTUS-4).

The VAWR thermistors measured water temperature at a depth of 0.6 m. On LOTUS-3, the VAWR thermistor was wired to a cable which extended around the buoy hull and along the rigid bridle; on LOTUS-4, the VAWR thermistor was attached to a cable which ran through the bulkhead and along the rigid bridle.

Relative Humidity

Accurate measurements of relative humidity are difficult to obtain close to the sea surface. The relative humidity sensor on LOTUS-4, HYCAL Engineering model HS-3552-B (Fig. 6), contains a hygromechanical strain-gauge beam. According to HYCAL Engineering document No. 76-867, the hygromechanical cellulose crystallite strip reacts to humidity in much the same manner as a bimetal strip reacts to temperature. A pair of piezo-resistive silicon strain-gauges are mounted on a stainless-steel beam. The bending of the hygromechanical strip strains the stainless-steel beam. The flat sides of the strain-gauge beam are shielded from the pressure of circulating air. According to the HYCAL document, this sensor has been used on ocean buoys with a typical full range accuracy of 6 percent. This level of accuracy seems optimistic for the LOTUS site. Salt accumulation on the sensor can have severe effects on the accuracy of the measurements (Payne, personal communication). This sensor, re-calibrated at WHOI, agreed with the manufacturer's linear calibration curve. The sensor was mounted on the tower, about 1.5 m above the waterline.

Solar Radiation

On LOTUS-3, solar radiation was measured with a HYCAL pyranometer, model P-8405-A. The detector is a differential thermopile with the hot junctions located at the receiving surface and the cold junctions directly behind. The sensor surface is blackened with a graphitic coating which absorbs more than 90 percent of incident shortwave radiation. The spectral range of the glass hemisphere is 0.35 to 2.5 microns. The sensor produces a voltage output that is proportional to incident solar radiation per unit surface area per unit time. Manufacturer's specifications:

Sensitivity: 5 mV/W m^{-2}

Linearity: $\pm$3 percent from 0 to 1400 W m^{-2}

Cosine Response: $\pm$1 percent for 0-70° zenith angle

On LOTUS-4, incident solar radiation was sensed with an Eppley Model 8-48 pyranometer (serial number 10420). The detector is a differential thermopile with the hot and cold junction receivers located on the element plate beneath the glass hemisphere. The hot junctions were blackened and the cold junctions whitened. A thermistor circuit in the sensor provides built-in temperature compensation. The glass hemisphere transmits energy between .285 and 2.8 microns. Manufacturers specifications:

Sensitivity: 11 mV/W m^{-2}

Linearity: $\pm$1 percent from 0 to 1400 W m^{-2}

Cosine Response: $\pm$2 percent for 0-70° zenith angle

$\pm$5 percent for 70-80° zenith angle

The accuracy of this sensor on a buoy is about 3 percent (Payne, 1974).

Previous experience with pyranometers mounted on WHOI deep-sea moored buoys indicated that neither buoy motion nor salt accumulation seriously degrades the data. The pyranometers were mounted on the tower at a height of approximately 3 m above the water. Data from the pyranometers were recorded on VAWR No. 184 (LOTUS-3) and No. 177 (LOTUS-4). After five months at sea, the glass hemisphere of the LOTUS-3 pyranometer was clean (Fig. 8).

Figure 8. Hycal pyranometer on LOTUS-3 after five months at sea.

Barometric Pressure

On LOTUS-3, barometric pressure was sensed with a high resolution Digiquartz pressure transducer manufactured by Paroscientific, Incorporated. The Digiquartz sensor (Paroscientific model 215A) utilizes a quartz crystal resonator whose frequency of oscillation varies with pressure-induced stress. Quartz crystals are used because of their insensitivity to temperature and their excellent stability. Overall accuracy of the Digiquartz pressure transducer is better than $\pm$ 0.2 mb over the range 0 mb to 1034 mb. The WHOI calibration curve is shown in Fig. 7. The Digiquartz sensor was sheltered from the dynamic pressure of the circulating air with a static pressure inlet developed by Gill (1976) (Fig. 6). The pressure port consists of two parallel plates oriented horizontally such that the air passes smoothly across the inside surface of the plates with the pressure sensing hole in its center. According to Gill (1976), the error of the pressure port is 0.5 mb at 20 m s^{-1} wind speed. The shield also protects the pressure sensor from radiation and sea spray. The accuracy of the sensor in the buoy environment is estimated at $\pm$ 0.5 mb. Two Digiquartz sensors were used on LOTUS-3; the data from one were recorded on VAWR No. 537 and data from the other were telemetered.

On LOTUS-4, a Digiquartz sensor was used and the data recorded on VAWR No. 381. Because of difficulties encountered during LOTUS-3 in interfacing the Digiquartz sensor with the satellite transmitter terminal, the more standard aneroid barometer was used for telemetry on LOTUS-4. The aneroid barometer (Yellow Springs Instrument Co., model 2014-28/32-HA-3-WH) uses an evacuated bellows to sense changes in absolute pressure. This change in pressure causes a proportional change in resistance which is measured by a potentiometer. According to the manufacturer, the accuracy is $\pm$.3 percent of the range span 28" to 32" Hg (948 to 1084 mb) or 3 mb.

The barometric sensors were mounted on the tower, approximately 2.5 m above the water.

Tension

The tensiometer, manufactured by William Swift, Co. of Bourne, Massachusetts, utilizes a hydraulic piston and cylinder filled with oil. Variable tension on the mooring line acts on the piston and changes the oil pressure. Higher pressure straightens a curved copper filament which is linked to the

moveable arm operating a resistance potentiometer. The potentiometer registers a resistance output proportional to the tension on the mooring line. The potentiometer has a 5 volt potential across it, corresponding to a range of 0 to 9300 lbs tension. The calibration curve, identical for LOTUS-3 and 4, is shown in Fig. 7. The tensiometer is located at the top of the mooring line, just below the rigid bridle. The data from the tensiometer were telemeterd on both LOTUS-3 and LOTUS-4.

IV. TELEMETRY SYSTEM

The ARGOS system consists of two polar-orbiting satellites with an orbital period of approximately 101 min. The orbits are inclined 98° and are sun-synchronous. Since the earth rotates about its polar axis, the satellite passes over a given latitude at a different longitude each orbit. The orbital plane of Satellite I is inclined 60° relative to that of Satellite II. Satellite I orbits at an altitude of 830 km $\pm$ 18 km, 40 km lower than Satellite II. Because of this, Satellite I has a slightly shorter period than Satellite II. Fig. 9 is a plot of the frequency and duration of satellite passes (more accurately of satellite data reception) over the LOTUS surface buoy during November 1982. The ordinate is year-days, the abscissa hours in the day. The two resulting diagonal patterns reflect the difference in angular velocity of the two satellites. (Satellite I, orbiting faster than Satellite II, generates the slightly shallower-slope pattern.) Note the absence of satellite coverage over the LOTUS area between the hours of roughly 02:00-05:00 and 14:30-16:30 UTC during November. The periods without satellite coverage change with the time of year.

The two ARGOS satellites together make an average of eleven passes every 24 hours over the LOTUS area. Each pass is about 10 minutes long. Fig. 9 shows that the frequency and duration of passes is somewhat variable.

An ARGOS Data Acquisition Platform (ADAP) onboard the LOTUS surface buoy transmits data to the ARGOS satellites by UHF radio. The ADAP terminal, manufactured by Polar Research Laboratories, is a portable self-contained unit measuring 41 cm x 41 cm x 41 cm. Selected meteorological and engineering sensors on the buoy are wired directly to the terminal. It can sample up to 16 sensors.

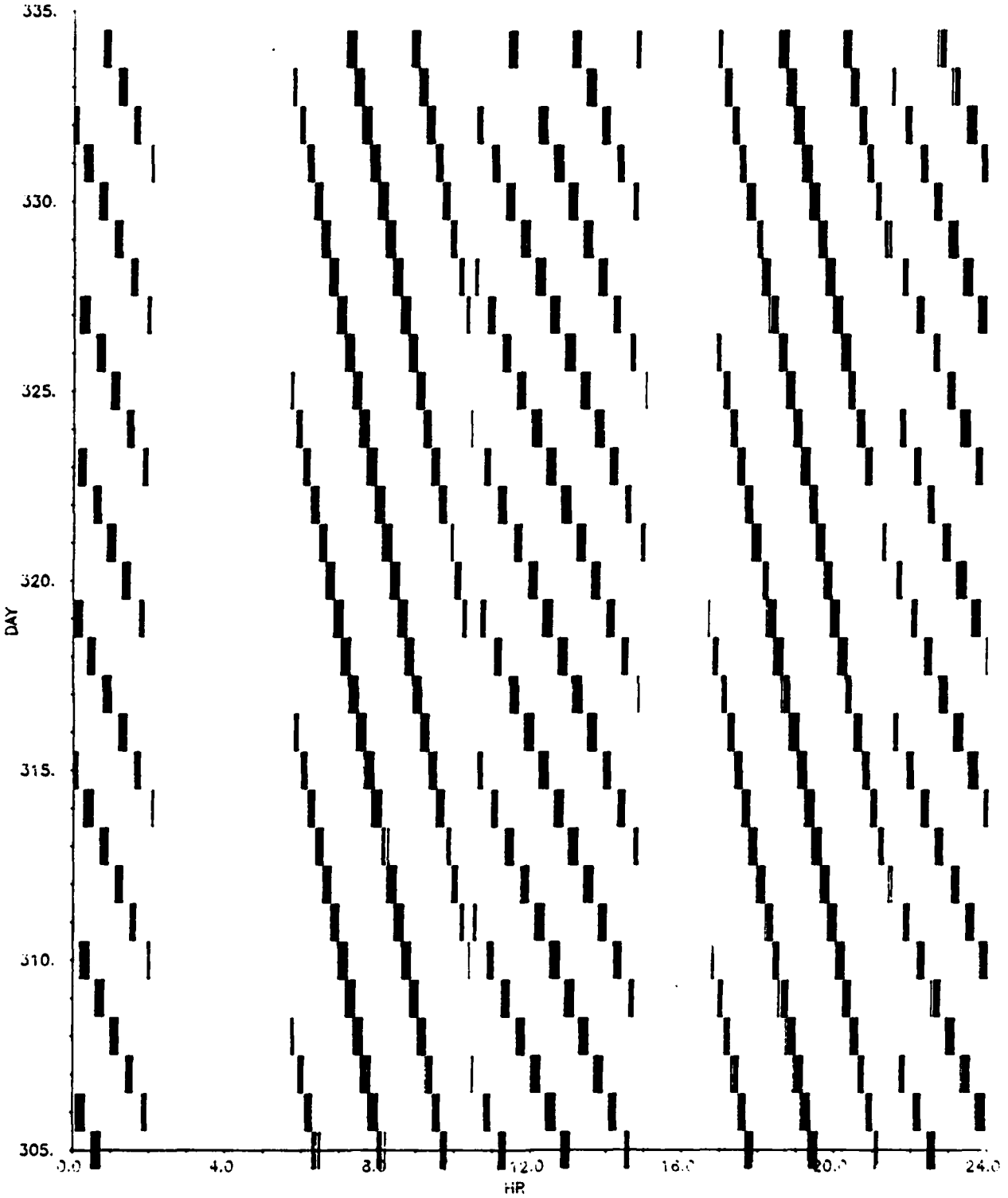

Figure 9. Frequency and duration of satellite passes over the LOTUS area. The abscissa is hours in the day in UTC, the ordinate is year-days. The lines mark the times the satellites received data from the buoy.

Fig. 10 is a schematic of the connection system. The sensor-terminal interface characteristics are given in Table 4. The terminal converts the analog voltage present at each sensor channel into an eight-bit digital word. The decimal count is related to the analog voltage input by

$$\text{Voltage input} = \frac{255}{5.0} \text{ decimal counts}$$

System resolution is therefore 19.6 millivolts per count.

The terminal samples its sensors and automatically transmits the data every 60 s $\pm$ 5 s at a frequency of 401.65 MHz $\pm$ 1.2 KHz. When the buoy is within the satellites' coverage, the data collection system onboard the satellite formats and stores the received data on tape and records the time and date of message reception. The data, buoy position, and time of each pass are read out once an orbit to a ground telemetry station. The data are then transmitted to the National Environmental Satellite Service (NESS) center in Suitland, Maryland, where they are separated out from data concerning other satellite systems. From NESS, they are transmitted to the CNES Toulouse Space Center in France where the ARGOS Data processing center is located. From France, the data are returned to Suitland where the most recent data (between 2 hours and 5 hours old) can be obtained by telephone. The data are also available monthly on 9-track magnetic tapes from the ARGOS data processing center.

Figure 11 shows an example of the ARGOS output obtained by telephone. The order of the parameters is given below:

1) Buoy identification number (1879 = LOTUS-3, 1878 = LOTUS-4)
2) Buoy position (degrees north, degrees west)
3) Satellite reception date of the sensor data (day from January 1, time in UTC)
4) Battery voltage for the meteorological sensors
5) Regulated battery voltage
6) Instrument well switch (0 = dry, 1 = wet)
7) Air temperature (degrees C)
8) Sea temperature (degrees C)
9) Mooring line tension (pounds)
10) Wind speed (m s^{-1})

11) Wind direction relative to buoy orientation (180° means wind vane is oriented parallel to buoy vane)

12) Buoy compass (degrees from magnetic north; compass plus relative wind direction minus 13° magnetic variation gives the direction the wind is coming from in degrees true)

13) Barometric pressure (hexadecimal counts on LOTUS-3, millibars on LOTUS-4)

14) Navigation light switch (0 = off, > 0 = flashing)

The telemetered data are used primarily for monitoring the buoy and the environmental conditions at the LOTUS site. The ARGOS System locates the buoy by measuring the Doppler shift on the carrier frequency of incoming messages. Figure 12 shows the position of the buoy during June and July as determined by the ARGOS location system. The accuracy of the ARGOS location system, 0.5 km rms, is shown as a scale. The line segments connect the positions between successive satellite passes. These excursions are on the order of two kilometers or less. Buoy motion is due to wind and currents; the currents are composed of mean flow, tides and inertial oscillations. During the summer, when winds were light, buoy displacements were mainly due to the mean currents.

A moored buoy is constrained to move within a circle centered at its anchor position whose radius is determined by the scope of the mooring line and the magnitude of the depth-integrated currents. During June, the buoy set north, northwest and southwest of its anchor position. During July, the buoy set east and southeast of its anchor. Thus, the buoy took two months to complete its watch circle. The westward displacement of the watch circle is due to the mean currents which LOTUS current meter records show are to the southwest.

Figure 13 shows the movement of the buoy from June to October. Superimposed on the position data are two watch circles which have been derived from a computer model of the buoy (based on Berteaux and Chhabra, 1973). For a specified current profile, the engineering model computes the drag and tension along the mooring line and the corresponding maximum excursion of the buoy. The inner watch circle is derived from a current profile of 20 cm s^{-1} at the surface with a decay rate as $z^{-0.07}$ to 10 cm s^{-1} at the bottom. The radius of this watch circle is 2.0 km. The 2 km watch circle was expected to encompass

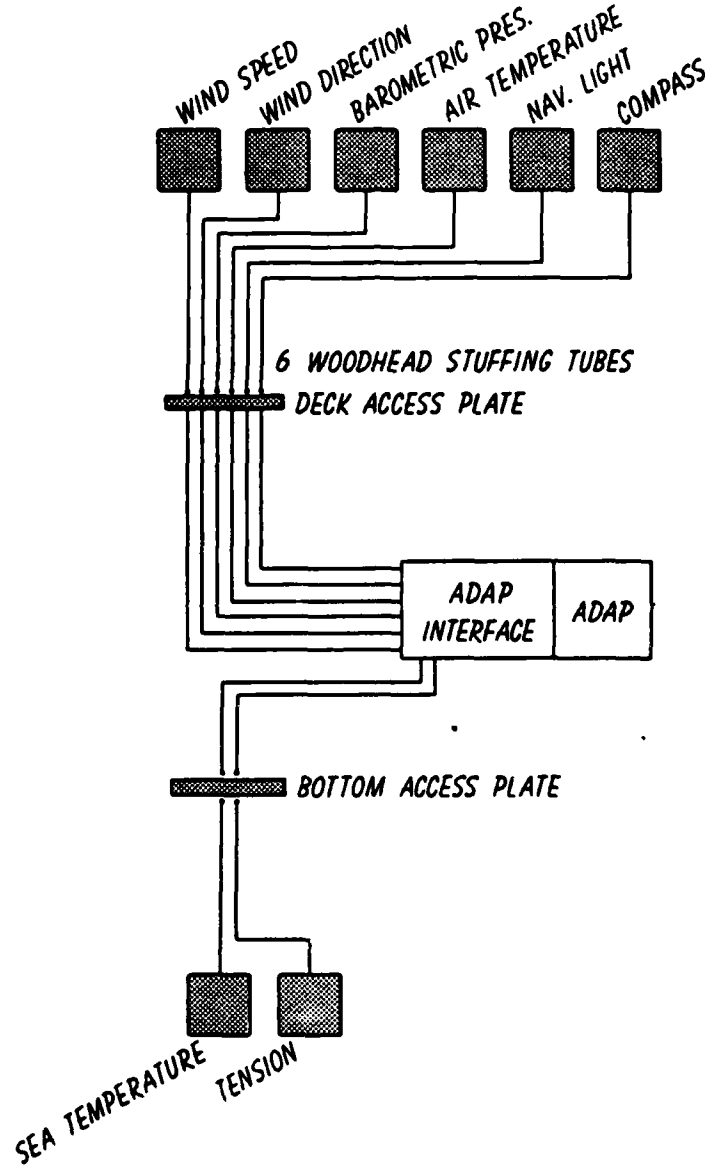

Figure 10. Schematic of the connections between the telemetered sensors and the ARGOS transmitter terminal (ADAP).

TABLE 4: SENSOR INTERFACE CHARACTERISTICS (LOTUS-3)

Channel		
1.	Battery Voltage	Scaling resistor, 0-5 v.
2.	Voltage Regulator Out	Scaling resistor, 0-5 v.
3.	Water Level	Float switch, series resistor, 0-3 v. (dry-wet).
4.	Air Temperature	Thermistor, 5°-40°C range, 0-5 v.
5.	Sea Temperature	Same as Channel 4, 14°-34° range, 0-5 v.
6.	Tension	Hydraulic pressure potentiometer, 0-5000 ohms for 0-9200 lbs. tension, 0-5 v.
7.	Wind Speed	Anemometer cups, DC generator, 0-5 v. for 0-100 MPH.
8.	Wind Direction	Shaft potentiometer, 0-360°, 0-5 v.
9.	Compass	(No interface necessary; part of basic sensor.)
10.	Barometric Pressure	Frequency-to-hexadecimal converter, to ladder resistor, to opamp, to analog, 0-5 v.
11.	Barometric Pressure	Same as Channel 10.
12.	Navigation Light Monitor	1-ohm photo-resistor in series with negative lantern battery terminal, 1.5 v. through RC integrator.

```
◆
EXP 0191

01878   33.960N  70.014W OR 43.837N 118.011W  007/0945Z-
 ( 1)   +.19024E+2  +.12000E+2  +.00000E+0  +.16678E+2
        +.20605E+2  +.26458E+4  +.30000E+0  +.20465E+3
        +.23993E+2  00          +.10190E+4  +.10588E+1
        00          00          00          E9

◆
EXP 0191

01879   33.961N  70.032W OR 31.803N  59.879W  207/0735Z-
 ( 1)   +.19106E+2  +.12059E+2  +.00000E+0  +.24746E+2
        +.25629E+2  +.22048E+4  +.15869E+1  +.19618E+3
        +.28227E+1  84          93          +.16471E+1
        +.00000E+0  00          00          00

ARGOS READY
◆
```

Figure 11. Example of the telemetered data accessed by phone from the National Environmental Satellite Service. Top: LOTUS-4. Bottom: LOTUS-3.

Experiment No.

Buoy ID	Actual lat. N	Actual long. W	irrelevant	year-day/time UTC
	Battery	Regulated	Well Switch	Air Temp
(Satellite No.)	Voltage	Voltage	(1=Wet,0=Dry)	(°C)
	Sea Temp	Mooring Line	Wind Speed	Wind Direction
	(°C)	Tension (lbs.)	(m/s)	(Degrees)
	Compass	-	Barometric	Light
	(Degrees)		Pressure	(0=Off,
			(mb LOTUS-4,	> 0=flashing)
			hex LOTUS-3)	
	-	-	-	-

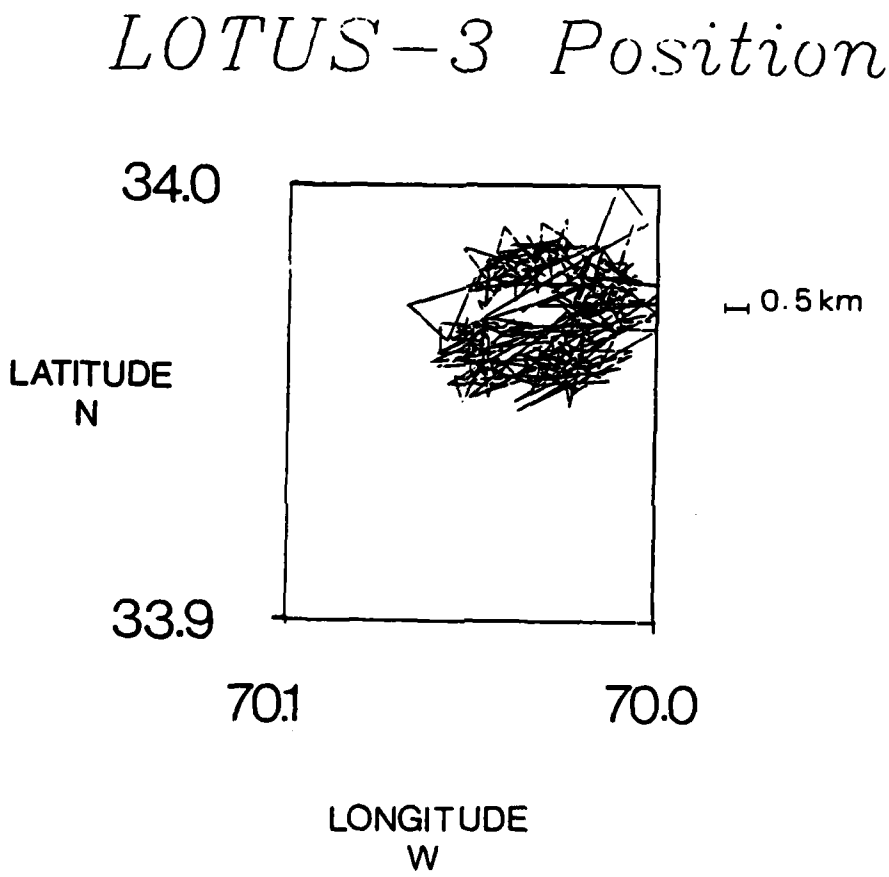

Figure 12. Position of LOTUS-3 during June and July 1982 as tracked by the ARGOS satellites. The accuracy of the positions, 0.5 km, is shown as a scale. The dot marks the anchor position. The lines connect the buoy position between successive satellite passes.

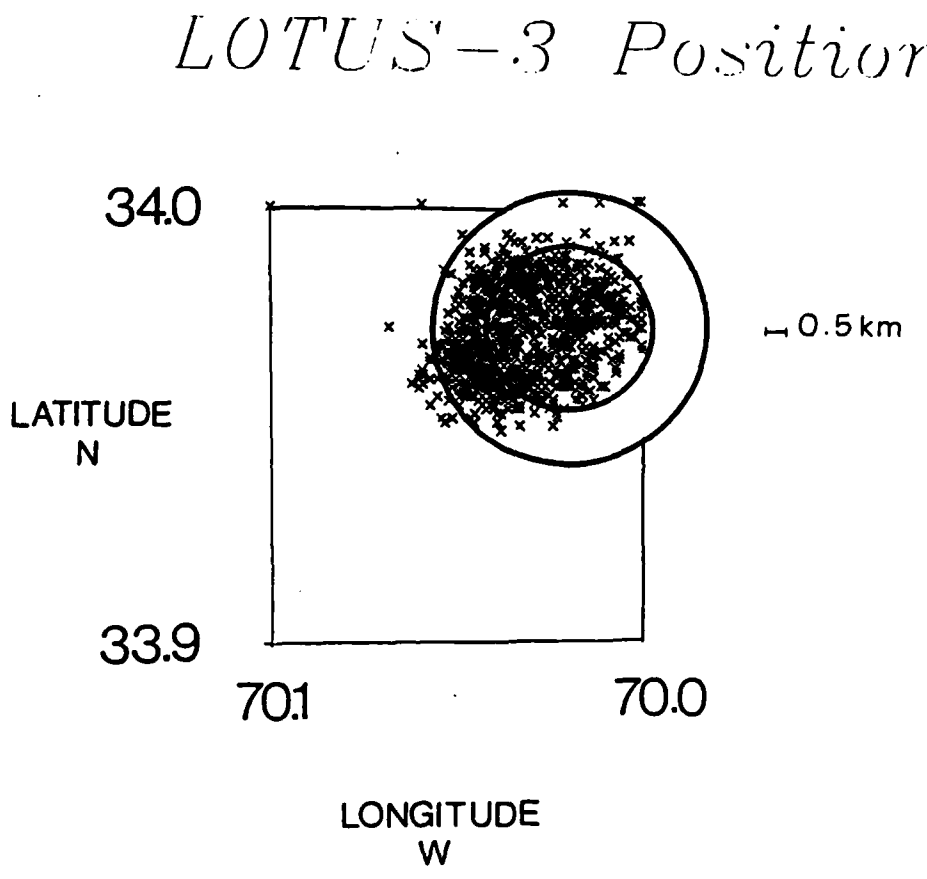

Figure 13. Position of LOTUS-3 during June to October 1982 as tracked by the ARGOS location system. The accuracy of the positions, 0.5 km, is shown as a scale. The watch circles (radii 3.45 km and 2.0 km) are centered at the anchor position. See text for explanation.

most of the buoy movement. The outer watch circle was derived from a current profile of 70 cm s^{-1} in the upper 500m with a $z^{-0.75}$ decay to 10 cm s^{-1} at the bottom. The radius of this circle is 3.45 km. This watch circle was expected to occur during the passage of a strong eddy or Gulf Stream ring through the LOTUS area. In fact, a strong eddy passed through the LOTUS site during the end of May. The tension increased to its highest value during deployment as the buoy set to its maximum excursion 3.5 km southwest of the anchor position. Surface currents increased to about 80 cm s^{-1} during this time. The sea surface temperature showed a large increase (3°C); current meter records indicated the water temperature signal was confined to the upper 40 m. This is probably the signature of a middle-aged Gulf Stream Ring at the LOTUS site.

The tracking capabilities of the ARGOS location system are critical should the mooring break loose. During the first engineering test deployment when the ARGOS location system was not being utilized, the LOTUS-1 surface mooring was lost. LOTUS-4 broke loose on February 18, 1983, was tracked using the ARGOS location system, and was successfully recovered 18 days later. Note that tension telemetry was also helpful, for it confirmed that sufficient weight was still hanging from the drifting buoy to keep the buoy stable to wave action, and that the subsurface instruments were still on it.

V. RESULTS FROM LOTUS-3

VAWR Data

LOTUS-3 was moored for 171 days from May 12 to October 30, 1982. VAWR #184 returned usable data from May 12 to October 21, 1982, 161 days. VAWR #537 returned data between May 13-August 22 and October 1-30 (101 + 30 days). Between August 23 and September 30, no data were recorded on the tape. Figures 14 and 15 present time series of all the data recorded on both VAWRs.

Telemetered Data

Figure 16 shows the time series of meteorological data telemetered via the ARGOS satellite system from May 12-October 30, 1982. The spikes in the data do not show real fluctuations. The time series of regulated battery voltage contains such spikes. Although the spikes are common, they rarely persist for more than one or two consecutive data transmissions.

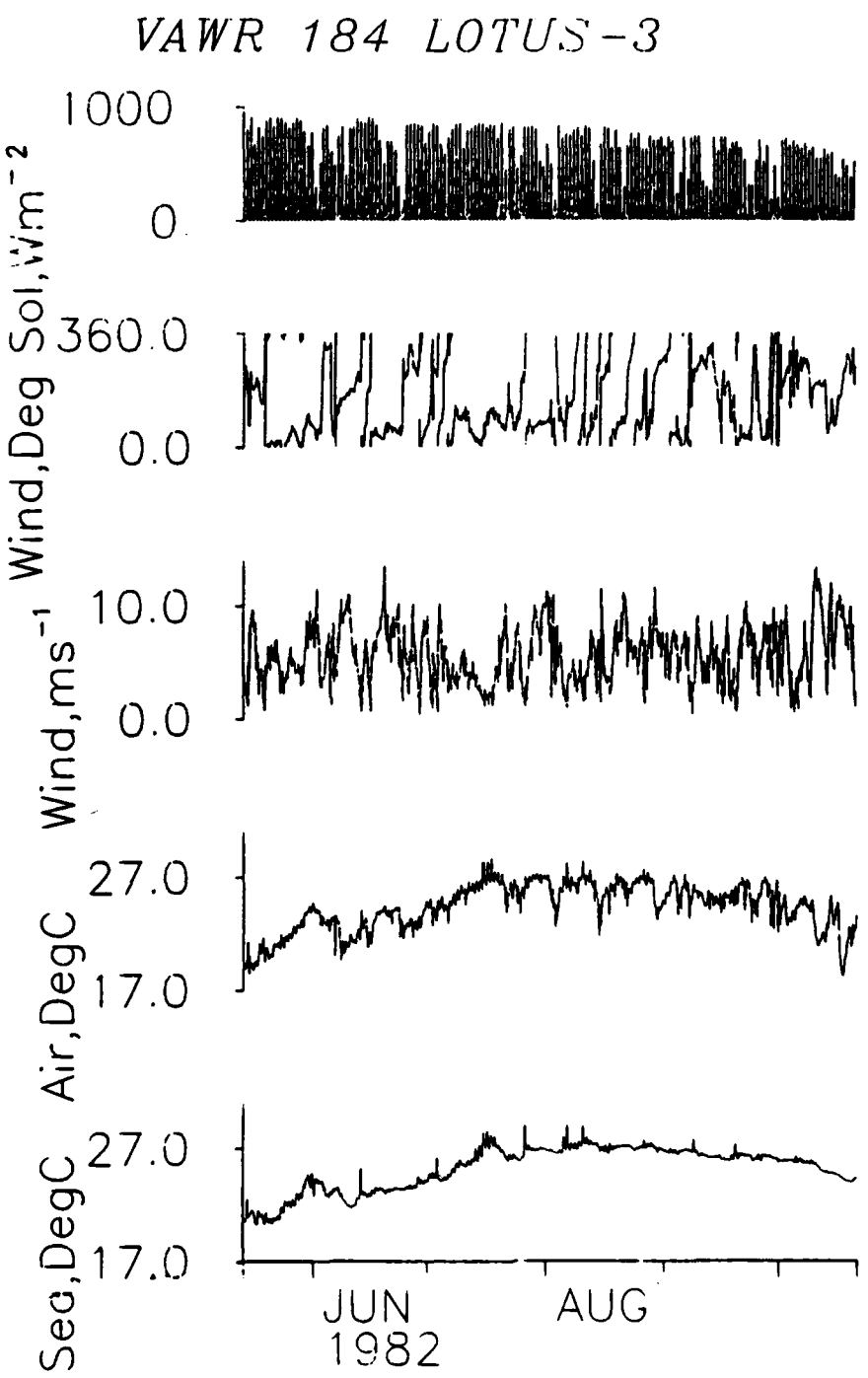

Figure 14. Time series of two-hour averages of sea and air temperature, wind speed and direction, and solar radiation from VAWR No. 184.

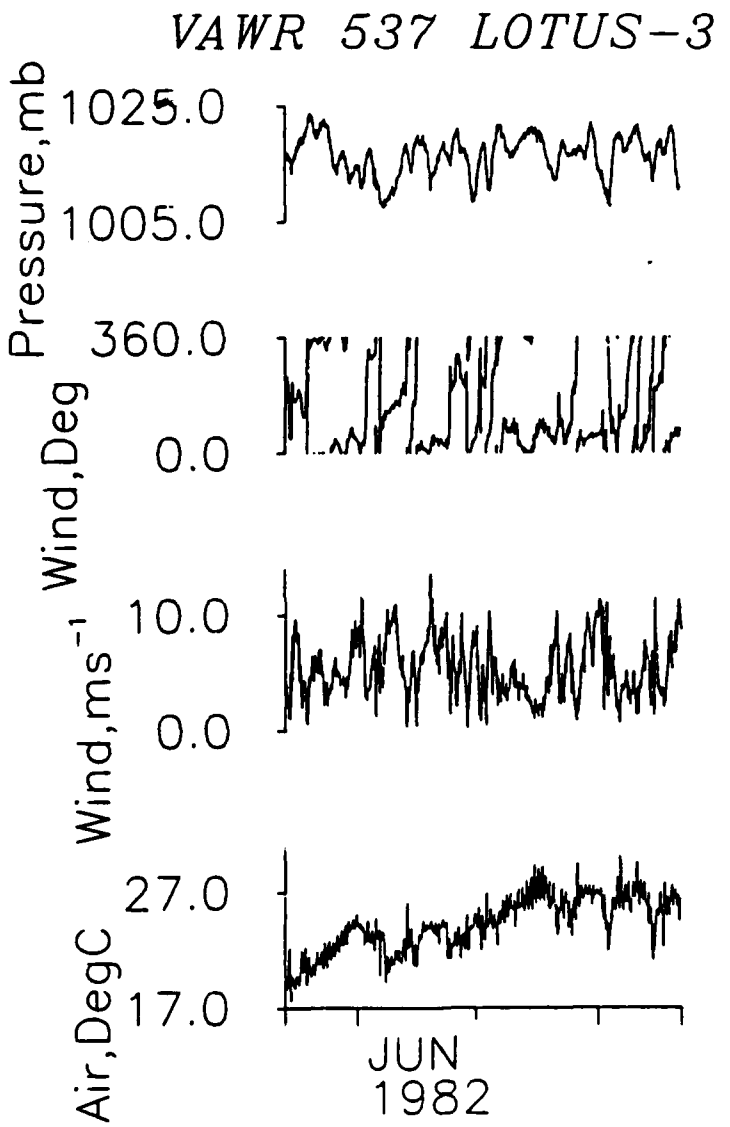

Figure 15. Time series of two-hour averages of sea and air temperature, wind speed and direction, and barometric pressure from VAWR No. 537.

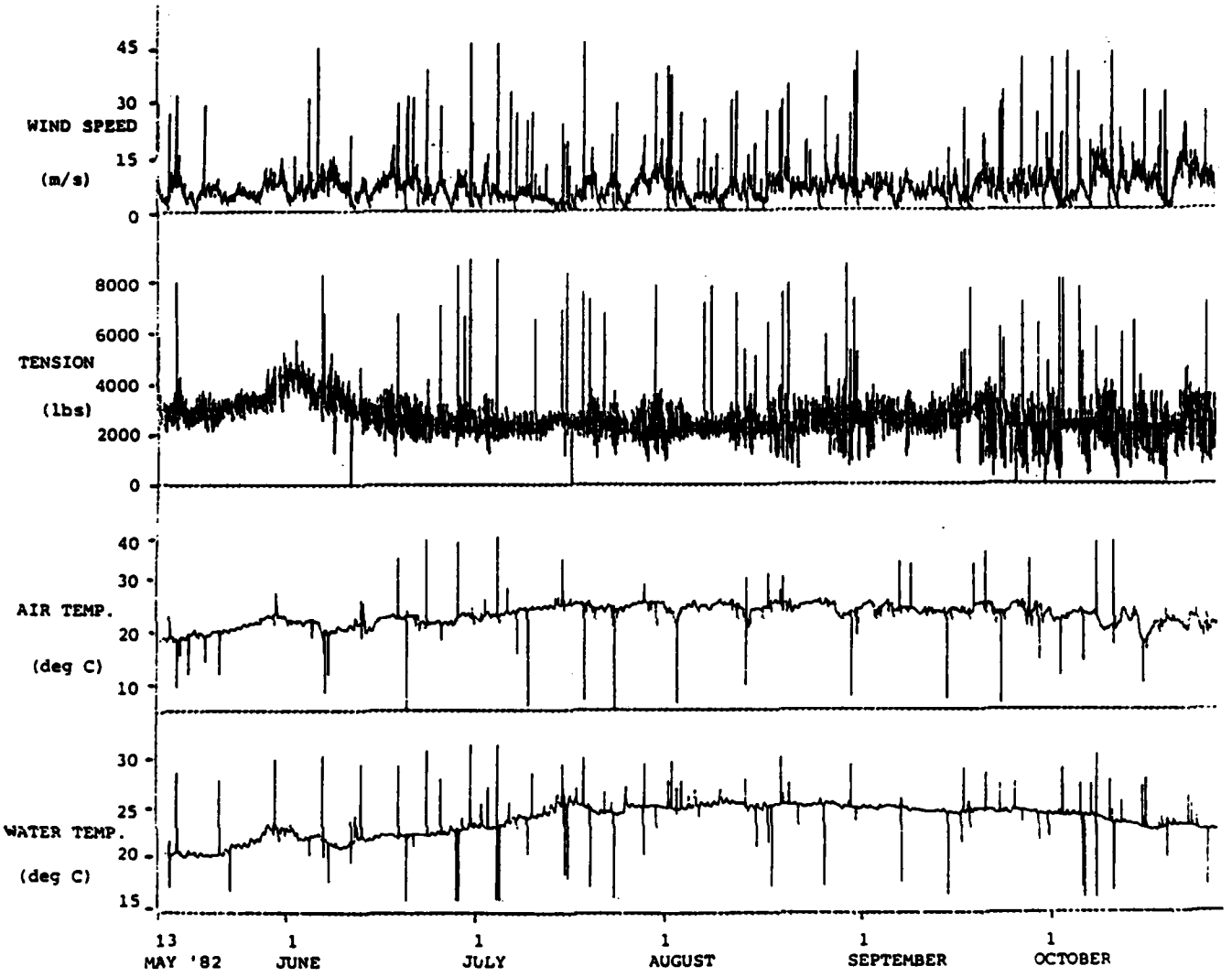

Figure 16. Unedited time series of telemetered sea and air temperature, tension along the mooring line, and wind speed.

To make the telemetered data more readily usable, all the data (excluding the spikes) collected during one pass of the satellite, about 10 minutes, were averaged for each variable. Data were rejected if they implied a fluctuation larger than a specified range. There were few borderline cases. A data set consisting of values at two hour intervals was obtained by making linear interpolations between the averaged values.

Figure 17 shows a comparison of the unedited and edited time series of air temperature. The two series are practically identical at time scales greater than an hour or two. Figure 18 shows the edited time series of the telemetered meteorological data. It is this time series which is used in the data comparisons with the two VAWRs that follow.

Tension along the mooring line was the only parameter that was telemetered but not recorded on a VAWR. Figure 16 shows the time series of tension; the tension record reflects the motion of the buoy. The high frequency fluctuations in the tension record are due to the jerky movements of the buoy as it rides the waves and swells. During periods of relatively high wind speeds, (e.g., July 27-Aug 6), the amplitude of the excursions in the tension record increases: we hope in later work to relate these excursions to measured wave-heights. During the period of high current (at the beginning of June) when the buoy was at its maximum excursion from its anchor, the tension was at its peak.

Sensor Comparisons

The data from redundant sensors are compared in scatterplots with regression lines and standard errors, differenced time series, and for winds, progressive vector diagrams. Unless stated otherwise, the VAWR data are averaged over two hour intervals in order to compare them with the telemetered data set. It should be noted that the telemetered data set cannot be as accurate as the VAWR data sets for two reasons: first, the digitization resolution of the data is better, by many orders of magnitude, for the VAWR sensors than for the telemetered sensors. For example, wind speed is resolved to 0.19 m s^{-1} on the telemetered wind sensor, and 8.3×10^{-4} m s^{-1} on the VAWR No. 184 wind sensor. Second, the telemetered data are collected only during satellite passes, or about eleven times a day for ten minutes per pass. Thus the telemetered sensors are not as well sampled in time as the VAWR sensors which are sampled every 3.75 minutes. However, the meteorological quantities change slowly

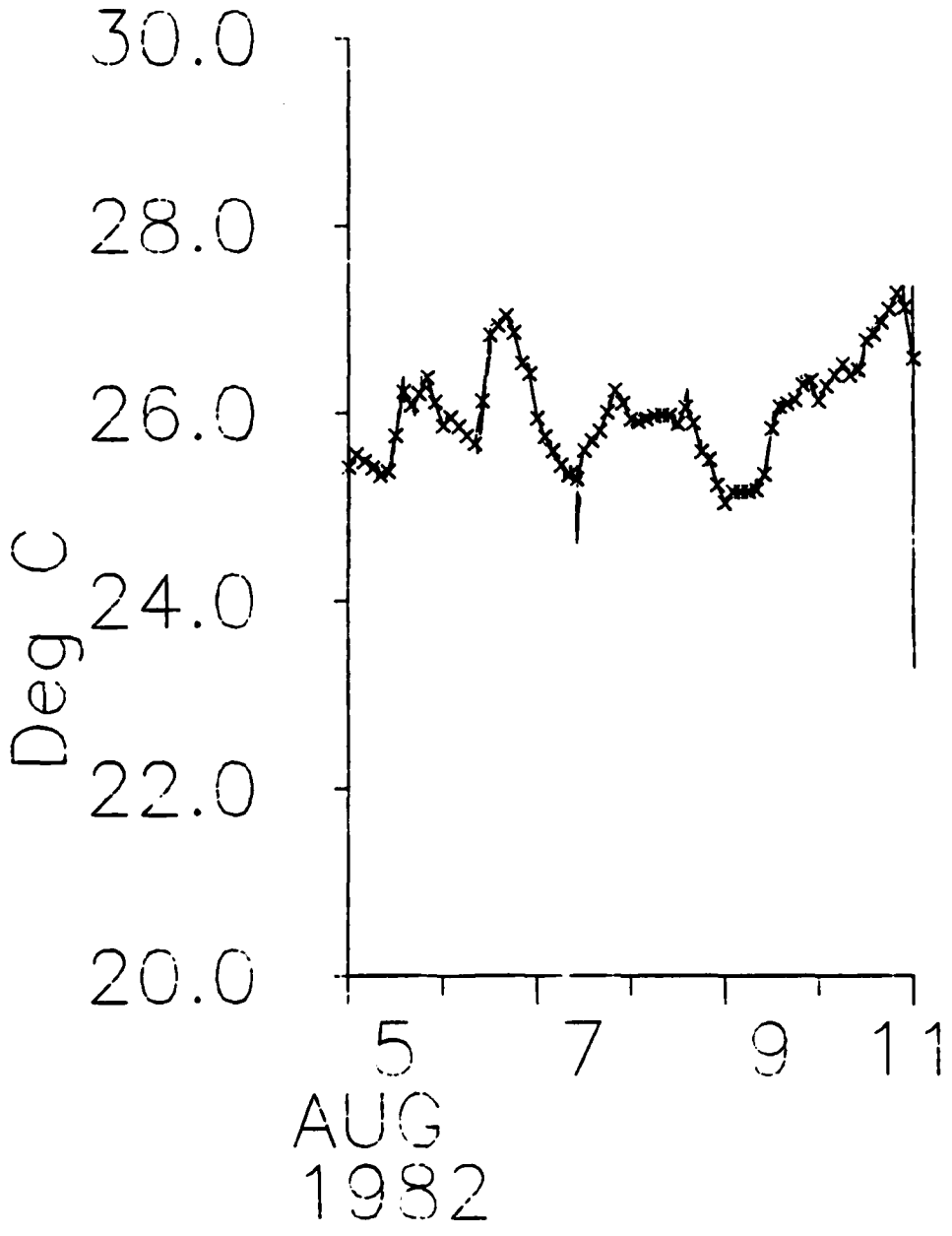

Figure 17. Comparison of the unedited and edited (X) time series of telemetered air temperature.

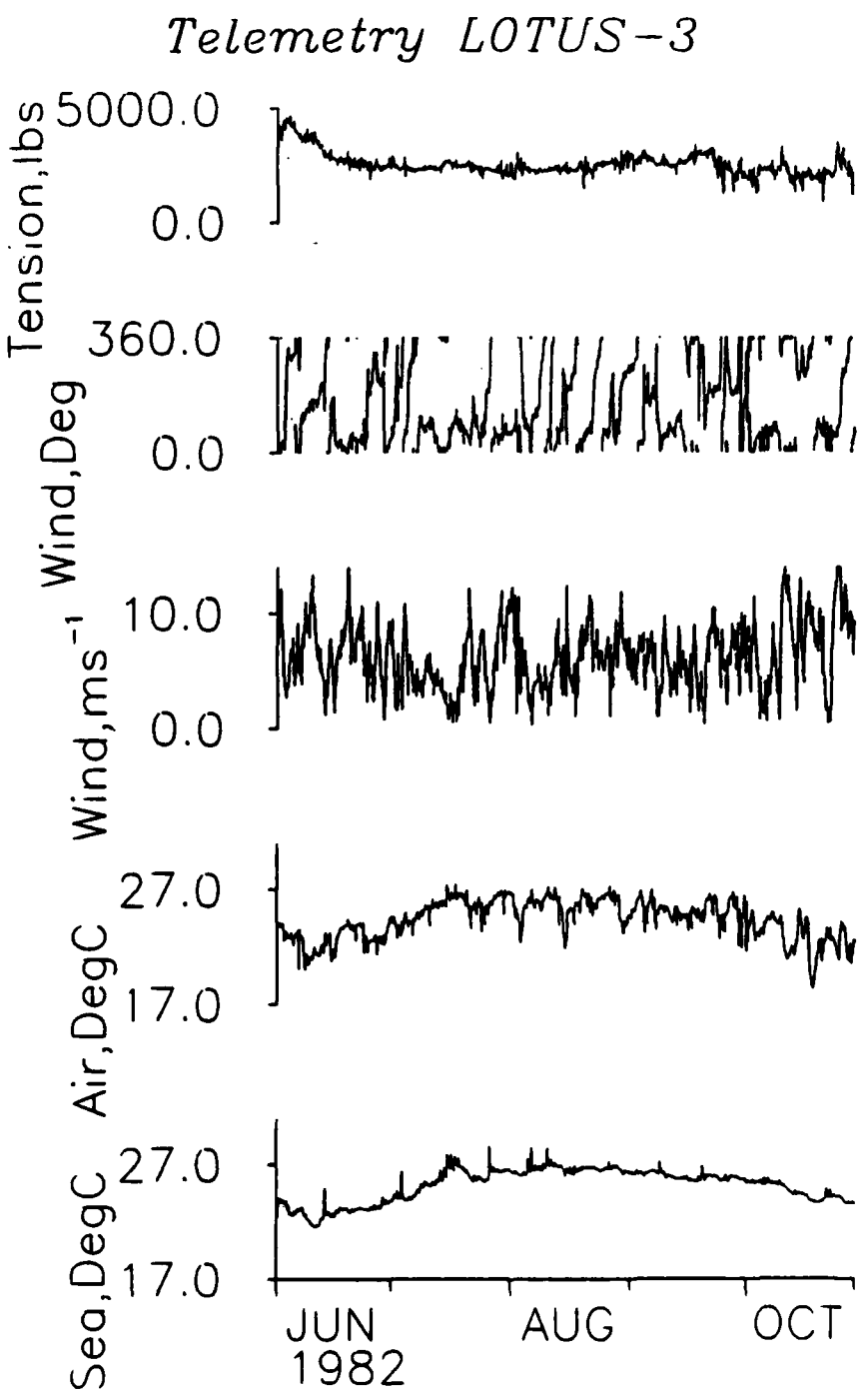

Figure 18. Time series of edited telemetered sea and air temperature, wind speed and direction, and tension along the mooring line.

enough that a ten minute sampling of the data compares well with a two hour average; this is equivalent to saying that little energy is contained in the short-period meteorological fluctuations compared to the longer-period fluctuations.

Wind Speed and Direction

Progressive vector diagrams of all three wind sensors are shown in Figure 19. The wind displacement vectors (two hour averages) are placed head-to-tail to show the path a perfect particle would have taken if the fluid were perfectly homogeneous with no spatial gradients. The telemetered Gill wind sensor and the VAWR No. 537 integral wind sensor compare well (within 5 degrees). The VAWR No. 184 Gill wind sensor appears rotated clockwise about 20 degrees with respect to the two other wind sensors. The offset changes by 5° at low bearings. The source of this wind direction offset has not yet been identified although it seems likely that there was an interference effect on the compass. The scatterplots of wind direction (Figure 20) show the VAWR sensors agree closely except for the 20° offset. The scatterplots of wind speed (Figure 20) show the VAWR sensors agree very well.

A "best" wind speed and direction time series has been constructed from the two VAWR wind sensors. The VAWR No. 184 Gill wind direction was rotated counterclockwise 20°. The last ten days from the VAWR No. 537 wind sensor data were appended to the rotated data set. The progressive vector diagram for this composite wind data is shown in Figure 21. Based on the comparison between the two VAWR sensors, the accuracy of the wind speed measurements is about 0.1 m s^{-1}, and that of wind direction about 5°.

Sea Temperature

Figure 22 shows time series of sea surface temperature measured by the telemetered and VAWR No. 184 thermistors. The telemetered thermistor actually measured the temperature of the base of the buoy hull; the VAWR No. 184 thermistor measured water temperature at a depth of 0.6 m. The hull temperature is 0.4°C lower, on average, than the water temperature. We can find no explanation for this mean offset.

Figure 22 shows the difference between the hull temperature and the water temperature. The temperature difference shows a small-amplitude (a few tenths of a degree) diurnal signal. At high temperatures, the temperature difference

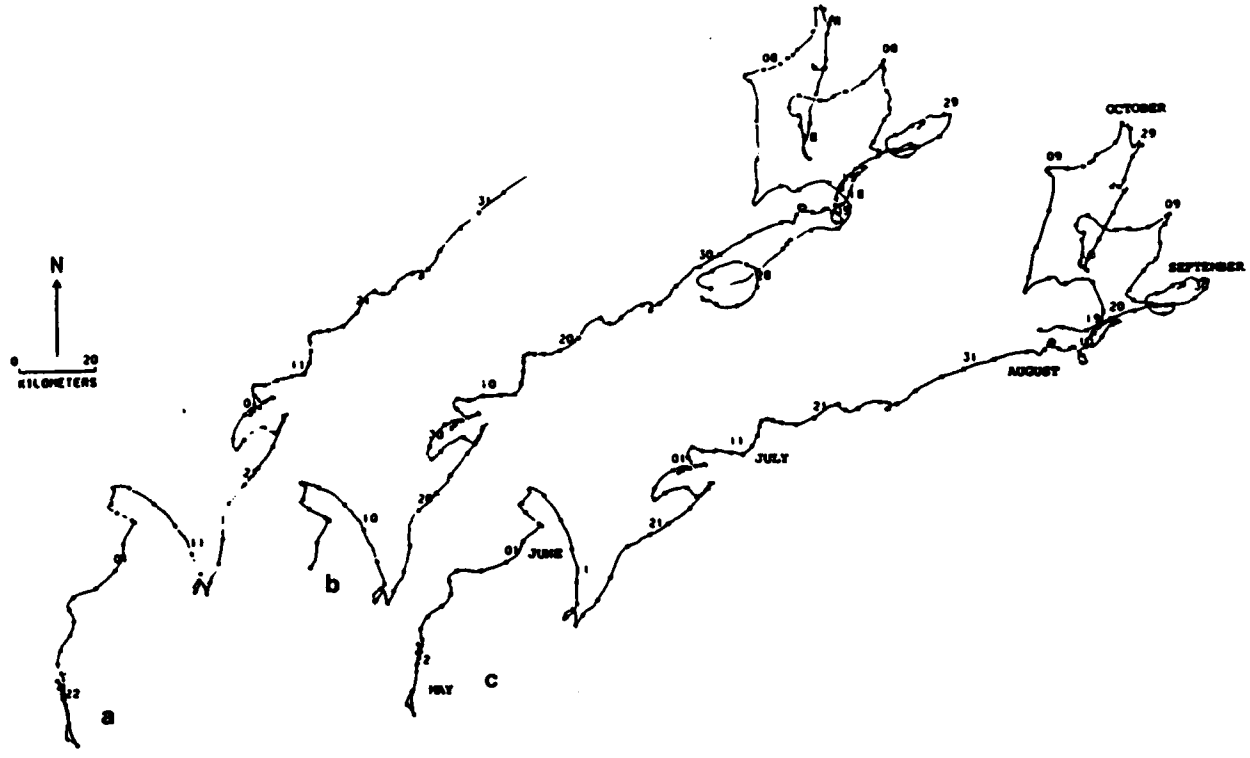

Figure 19. Progressive vector diagrams of winds from (a) VAWR No. 537, (b) telemetry, (c) VAWR No. 184.

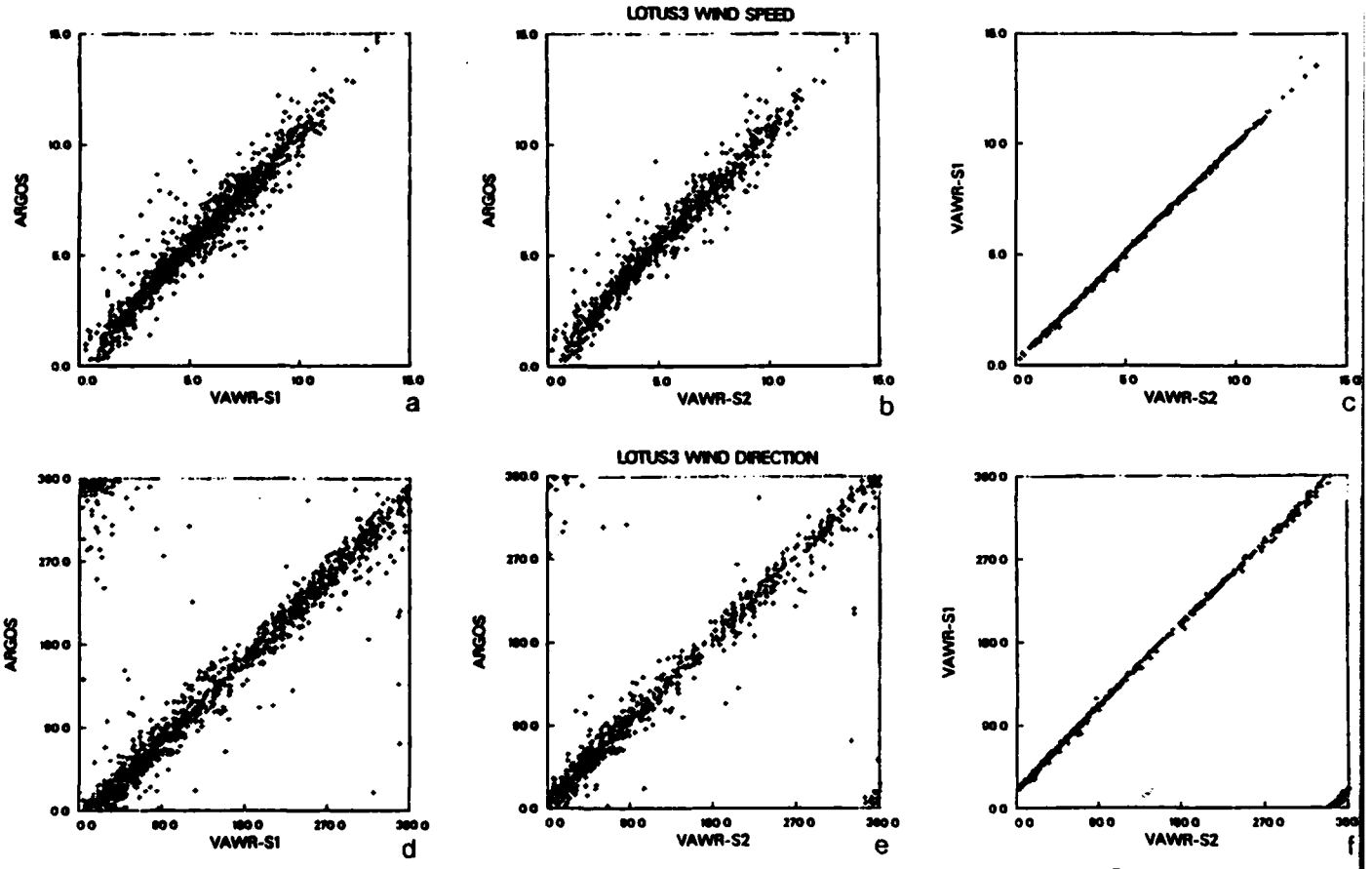

Figure 20. Scatterplots of two-hour averaged wind speed and direction from the three wind sensors on LOTUS-3. See Table 5 for the regression statistics.

TABLE 5: Index to Scatterplots (Y = A + Bx)
for LOTUS-3, 2-hour averaged data

Figure	Variable	Y-axis	X-axis	Units	A	Standard Error	B	Correlation Coefficient
20 a	Wind Speed	ARGOS	VAWR 1	m s^{-1}	0.06	1.060	0.924	0.976
b	Wind Speed	ARGOS	VAWR 2	m s^{-1}	-0.02	1.063	0.930	0.976
c	Wind Speed	VAWR 1	VAWR 2	m s^{-1}	-0.08	1.008	1.006	1.000
d	Wind Direction	ARGOS	VAWR 1	deg	45.85	(954.3)	0.6047	0.672
e	Wind Direction	ARGOS	VAWR 2	deg	20.18	(1092.0)	0.811	0.788
f	Wind Direction	VAWR 1	VAWR 2	deg	30.79	(965.6)	0.750	0.656

NOTE: VAWR 1 refers to VAWR #184
VAWR 2 refers to VAWR #537
ARGOS refers to telemetered data

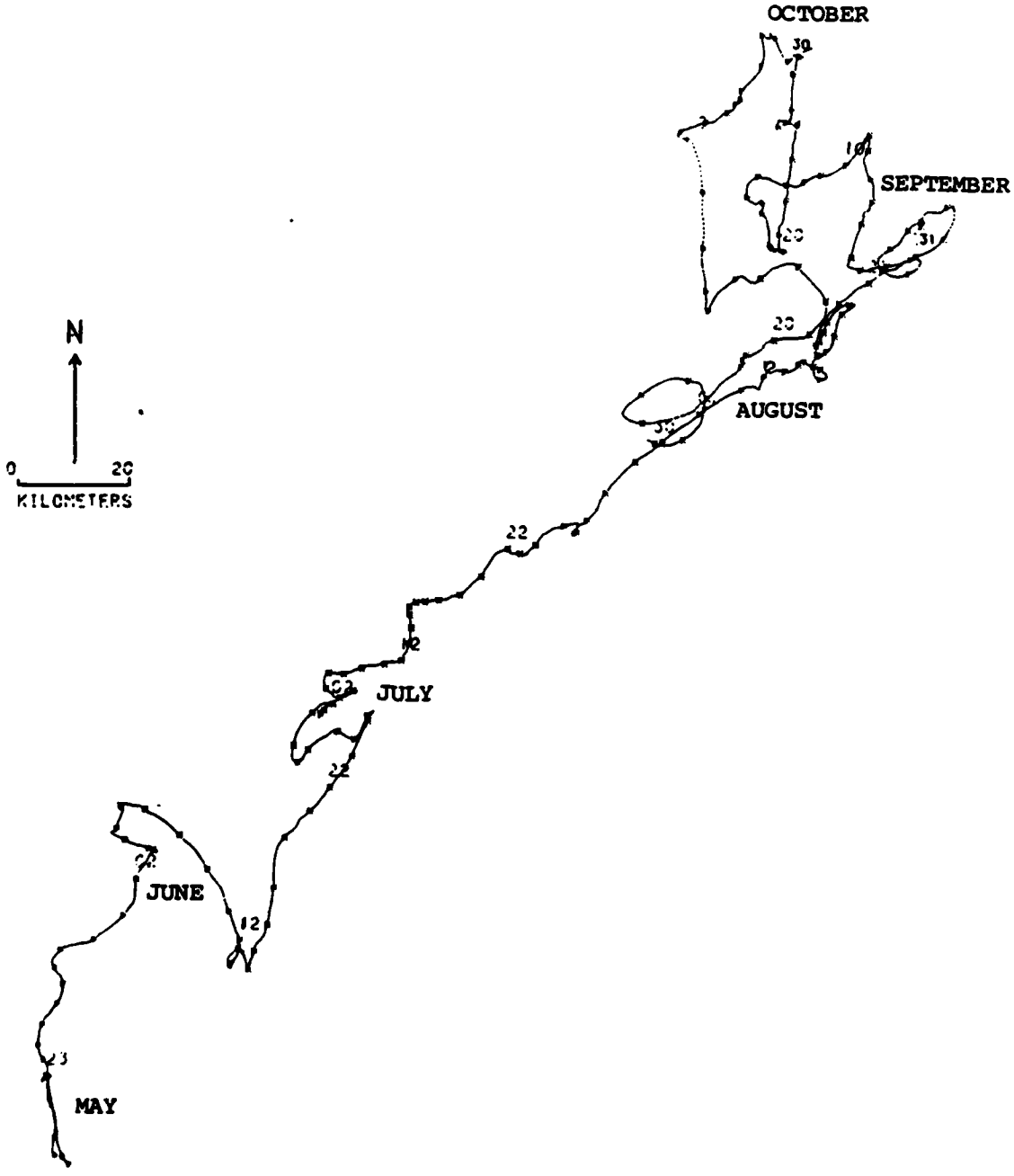

Figure 21. Progressive vector diagram of "composite" wind.

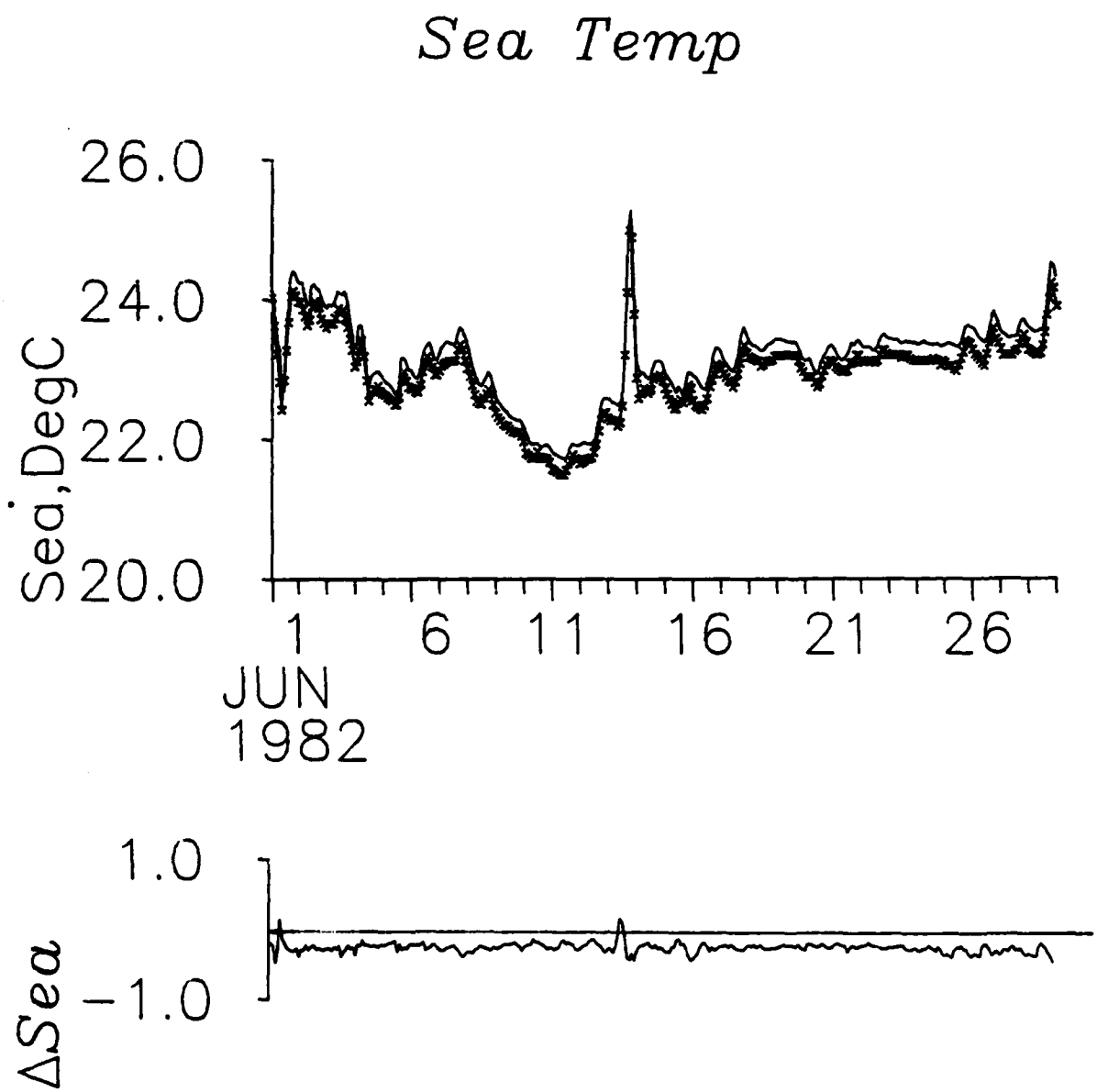

Figure 22. (a) Time series of hull (X) and sea temperature during June 1982. (b) Time series of hull minus sea temperature during June 1982, from LOTUS-3.

increases (relative to the mean offset) (Figure 23). The diurnal signal of the temperature difference is probably the effect of radiational heating and cooling on the aluminum hull.

Air Temperature

Figure 24 shows the time series of air temperature measured by the telemetered and VAWR sensors. The telemetered and VAWR No. 184 air temperature sensors identical Thaller-shielded thermistors. The VAWR No. 537 sensor is a PRL-housed thermistor. The two Thaller-shielded thermistors agree to within the sensor accuracy (0.3°C). The PRL-housed thermistor shows the effects of radiational heating. The difference time series between the PRL and Thaller-shielded thermistors, shown in Figure 24, has a strong diurnal cycle. On sunny, calm days, the PRL-housed thermistor heats up 1°-2°C above the Thaller-shielded thermistor. The scatterplot between the two VAWR sensors (Figure 23) shows most of the scatter occurs when the PRL housing heats up.

Barometric Pressure

The data returned from the telemetered barometric pressure sensor were physically unreasonable, fluctuating as much as 100 mb in one day; therefore, they were rejected. The circuit interface between the sensor and the telemetry system is suspect.

Solar Radiation

Measurements of insolation are very important to the calculation of the energy budget of the mixed layer. The data returned from the pyranometer on LOTUS-3 show two unresolved problems:

1) Nighttime (non-zero) trend (Figure 25a): there was an average nightly gain of 5 W m^{-2} increasing to 10 W m^{-2}. On certain nights the gain was much greater (about 30 W m^{-2}). We suspect this was caused by a drift in the circuitry or a temperature sensitivity (J. Dean, personal communication). The measured average nightly insolation represents only about 3 percent of the average daily insolation, however, and has been neglected.

2) Constant Offset: the insolation measurements appear to underestimate the amount of shortwave radiation by about 60 W m^{-2}. Figure 25b compares the observed insolation with the calculated insolation under clear skies based on latitude and solar altitude (Seckel and Beaudry, 1973). This comparison suggests that skies were never clear at the LOTUS site between May and October.

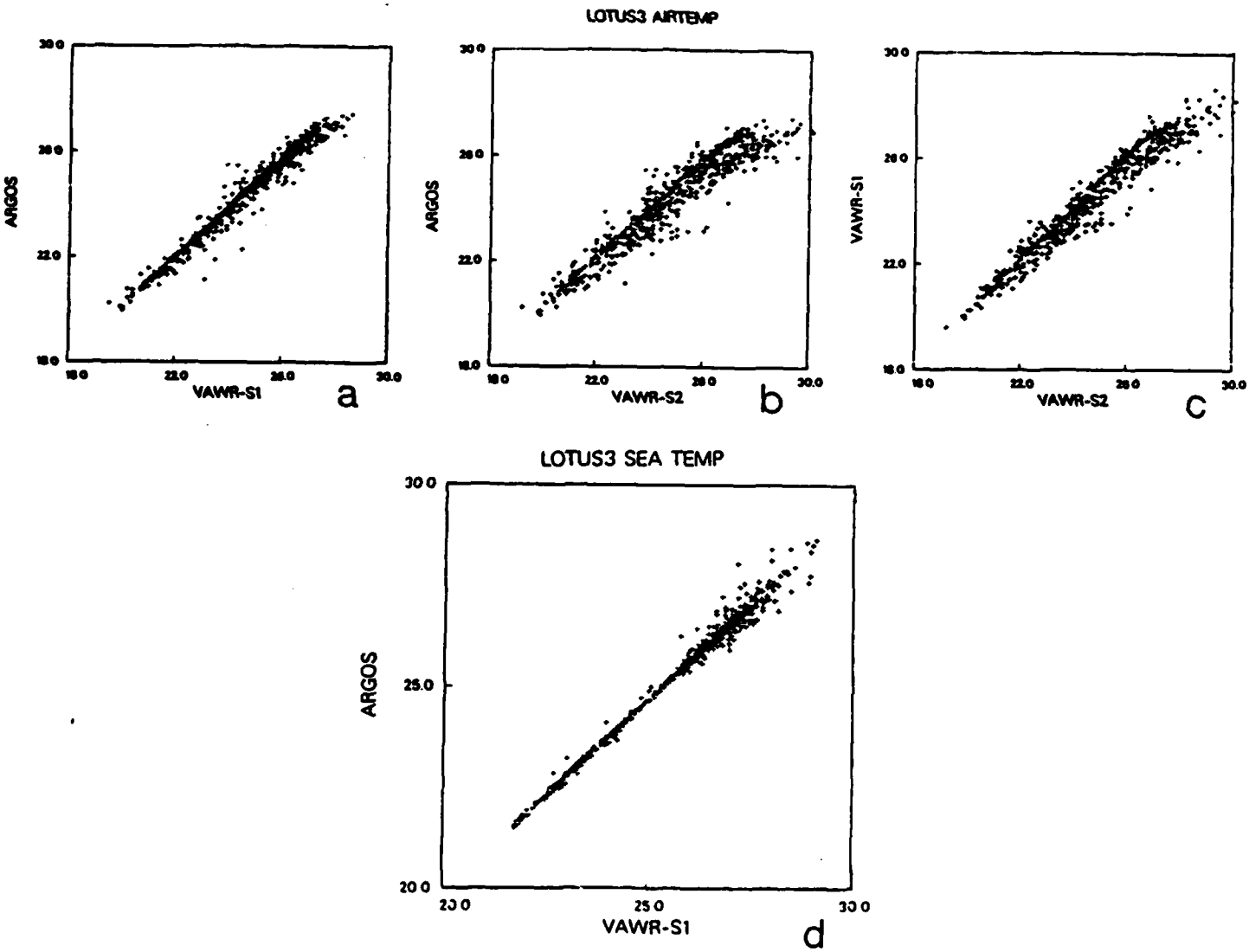

Figure 23. Scatterplots of two-hour averaged air and sea temperature from LOTUS-3. See Table 6 for the regression statistics.

TABLE 6: Index to Scatterplots (Y = A + Bx)
for LOTUS-3, 2-hour averaged data

Figure	Variable	Y-axis	X-axis	Units	A	Standard Error	B	Correlation Coefficient
23 a	Air Temperature	ARGOS	VAWR 1	°C	-1.555	2.730	1.075	0.990
b	Air Temperature	ARGOS	VAWR 2	°C	-2.940	2.854	1.114	0.954
c	Air Temperature	VAWR 1	VAWR 2	°C	-1.553	3.001	1.068	0.973
d	Sea Temperature	ARGOS	VAWR 1	°C	-0.821	2.816	1.047	0.997

NOTE: VAWR 1 refers to VAWR #184
VAWR 2 refers to VAWR #537
ARGOS refers to telemetered data

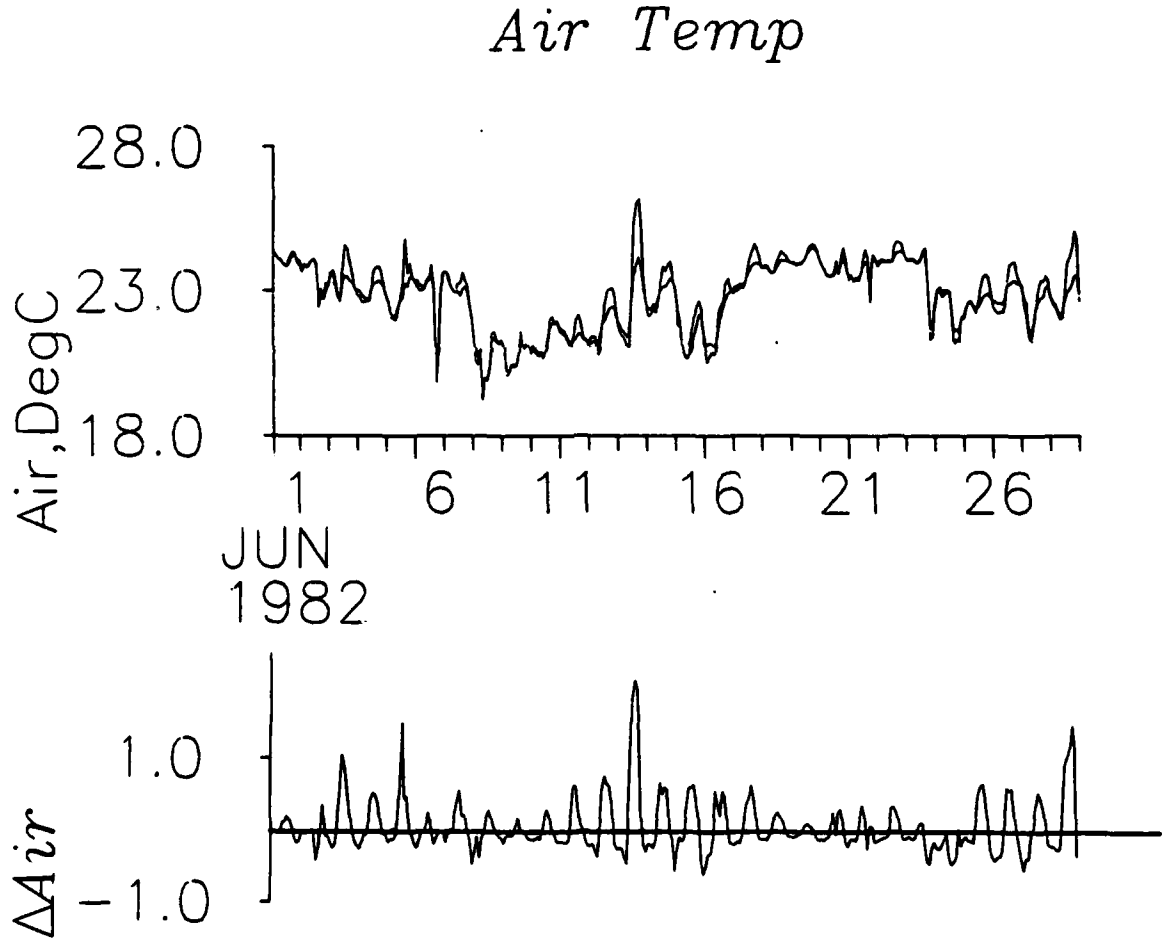

Figure 24. (a) Time series of air temperature from the Thaller- and PRL-shielded thermistors. The PRL housing overheats by 1°C-2°C during calm, sunny days. (b) Air temperature difference, during LOTUS-3.

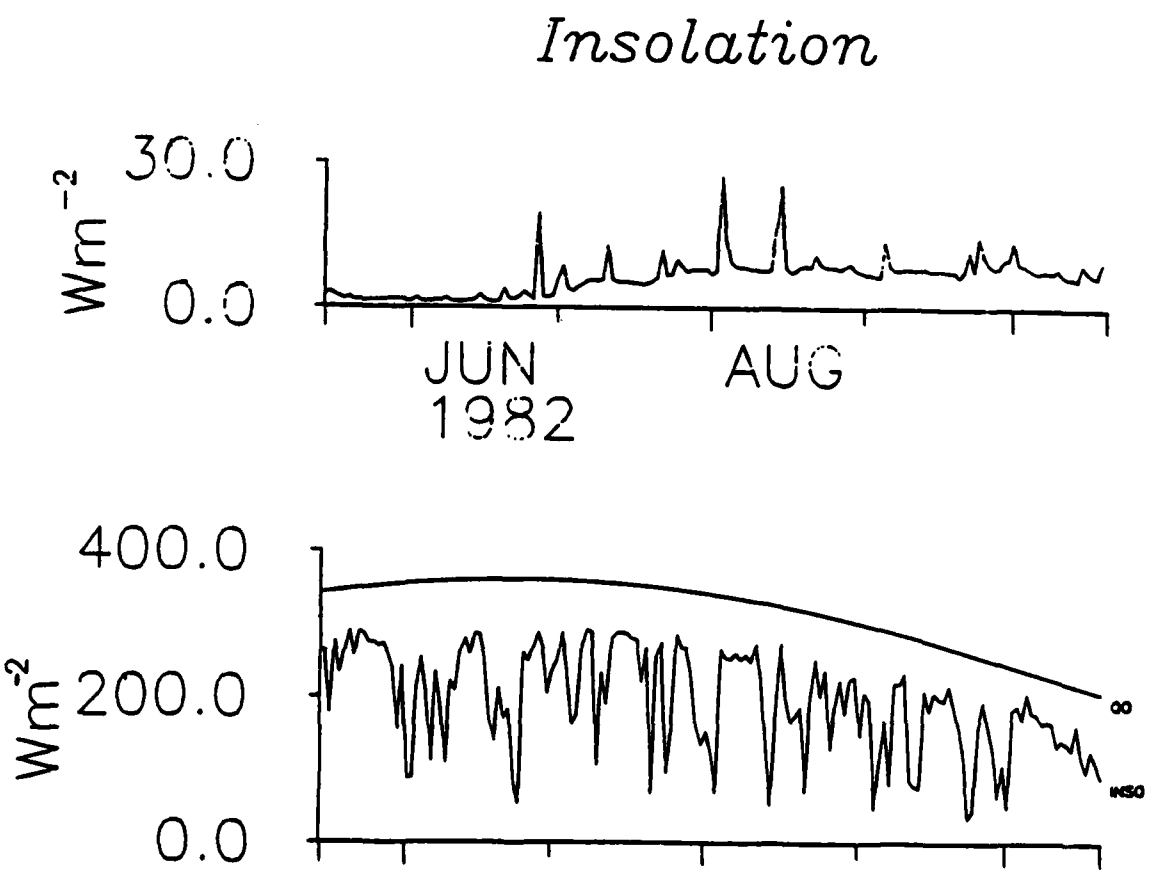

Figure 25. (a) Nightly-averaged solar radiation in W m^{-2} from LOTUS-3. (b) Comparison of clear-sky (QO) and measured (INSO) insolation.

In fact, according to the cloud reduction factor used by Reed (1975, 1977) (see Appendix), the clearest skies during this period were four-tenths covered by clouds. We have personally observed some completely sunny days during this period, however. Shadowing of the sensor by the buoy structure may have occurred at times.

For this reason, the insolation data from LOTUS-3 are still tenuous. (LOTUS-4 insolation data are much improved in this respect.) Where the LOTUS-3 insolation data are used in estimating the net heat exchanged between the air and the sea surface, they have been augmented by 60 W m^{-2}, which brings the LOTUS curve in Figure 25b up against the Seckel and Beaudry curve as a limit.

VI. HEAT FLUXES

One of the goals of the LOTUS experiment is to describe the heat content of the mixed layer over a two-year period. The heat content of the mixed layer at a site can be determined by calculating the heat exchanged with the atmosphere and measuring the amount of heat advected by currents and eddies into and out of the area. The LOTUS moored array provides temperature profiles from which the temperature and depth of the mixed layer can be computed. The current data returned from LOTUS will be used to determine the advection of heat in the mixed layer. The meteorological data collected from the LOTUS surface buoy are used for calculating the heat exchanged between the sea surface and the atmosphere.

Bulk formulas are used to estimate heat fluxes (net longwave radiative, latent, and sensible) at the sea surface.

The net heat flux at the sea surface is:

$$A = Q_S (1 - \alpha) - IR - S_E - L_E$$

where Q_S is the shortwave solar radiation

α is the albedo

IR is the net longwave radiation

L_E is the latent heat flux

S_E is the sensible heat flux

We have tried to be consistent with Bunker (1975, 1976) in our heat flux notation.* Details of the bulk formula parameterizations are given in the Appendix. The calculation of the latent heat flux deserves mention here. Since water vapor data were lacking during LOTUS-3 and most of LOTUS-4, the latent heat flux was estimated using the Bowen ratio method:

$$L_E = S_E/B$$

where

B is the Bowen ratio.

Bowen ratios have been determined from 32-year monthly-mean sensible and latent heat fluxes in the LOTUS area computed by Bunker (Bunker, 1975; Bunker and Goldsmith, 1979; Goldsmith and Bunker, 1979). The Bowen-ratio method has been questioned but the following analysis shows the monthly-averaged latent heat flux can be determined surprisingly well from the Bowen ratio.

LOTUS-4 provided relative humidity data during November 1-22, 1982. These data have been used in the bulk formula to calculate a mean latent heat flux during November of 120 W m^{-2} (see Appendix for details). The mean latent heat flux estimated from the Bowen ratio for November is 123 W m^{-2} $\pm$ 63 W m^{-2}. It should be noted that the monthly-averaged Bowen ratios cannot be used to calculate daily latent heat fluxes: the standard deviation of the daily Bowen ratios calculated from November 1-22, 1982, is as large as the mean ratio itself. Thus we are constrained by our use of monthly-averaged Bowen ratios to compute the net heat flux between the air and the sea on a monthly, and not daily, basis.

Figure 26 shows the heat fluxes computed from measurements made during LOTUS-3 and LOTUS-4, May 15, 1982, to March 3, 1983. Monthly-averaged heat fluxes are computed from two-hour averages of the observed quantities. The net heat flux residual shows an annual cycle: between May 15 and October 1, the ocean gains heat from the atmosphere and after October 1 the ocean loses heat to the atmosphere. The air temperature becomes progressively cooler than the water temperature after August 1. As a result of the increasing temperature gradient between the sea surface and the air above it, the flux of sensible heat from the sea to the air increases from approximately 0 to 80 W m^{-2} from

---

* See also the NOTE at the beginning of the References.

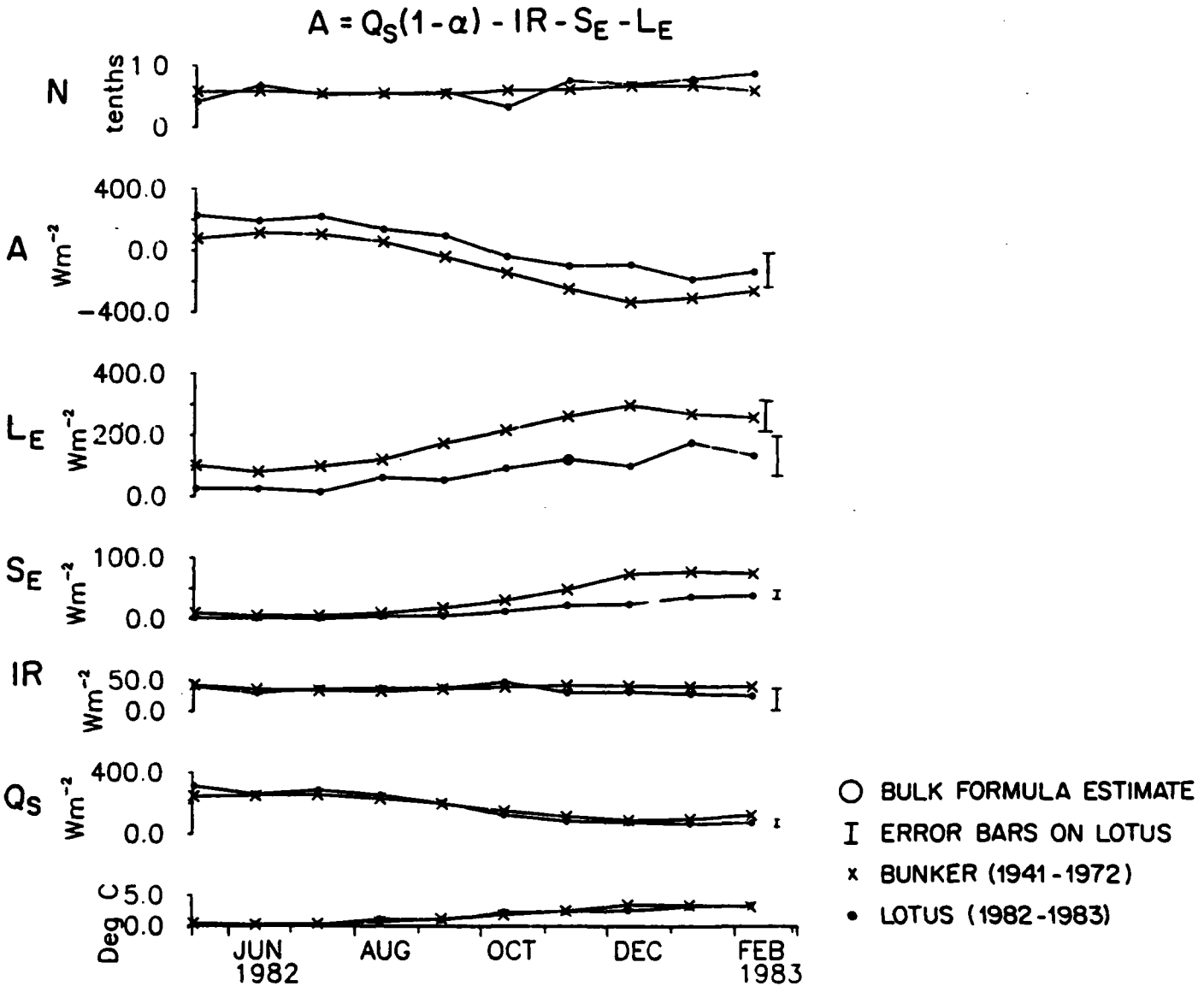

Figure 26. Comparison of heat fluxes from the monthly-averaged LOTUS data (•) and from Bunker's 32-year monthly means (X) (Bunker, 1975). From the top, N is cloud cover, A is net heat gain/loss by the ocean, L_E is latent heat flux, S_E is sensible heat flux, IR is net longwave radiation flux, Q_S is solar radiation, and sea minus air temperature.

summer to winter. Note that since the difference between the air and sea temperature is always greater than or equal to zero, the sensible heat flux represents a heat loss from the ocean. Since (using Bowen ratios) the latent is scaled by the sensible heat flux, the latent heat flux also increases from summer to winter, although the proportion of latent to sensible heat flux decreases. Solar radiation decreases from 300 W m^{-2} to 70 W m^{-2} from summer to winter.

The errors in the heat flux terms have been estimated from errors in the measured parameters. From scatter plots, the accuracy of the air temperature data is about 0.3°C, water temperature 0.01°C, wind speed 0.1 m s^{-1}, drag coefficient 0.2 x 10^{-3}; the accuracy of the Bowen ratios is given in the appendix. Corrections for height and stability may introduce additional large errors to the heat fluxes but have been left out. The expected errors in the heat flux are estimated to be:

Solar radiation flux, $Q_s(1 - \alpha)$: 16 W m^{-2},
net longwave radiative flux: 25 W m^{-2},
sensible heat flux: 9 W m^{-2},
latent heat flux: 63 W m^{-2}.

Summing the errors of the individual flux terms gives a total expected error of about 113 W m^{-2}.

The largest source of error in the surface heat flux is the latent heat flux term calculated from the Bowen ratio; it represents over 50 percent of the expected error in the net heat flux. The expected error in the latent heat flux changes very little from month to month: although the Bowen ratios show less scatter (standard deviation/Bowen ratio) during November and December, the large air-sea temperature difference during the winter compensates.

The importance of accurate humidity measurements for determining the heat exchange at the air-sea interface is demonstrated in this analysis. LOTUS-5 and LOTUS-6 are designed to provide relative humidity data so that the heat budget can be calculated more satisfactorily.

Bunker has calculated monthly-averaged heat fluxes using 32 years of ship's weather reports from the LOTUS area (Bunker, 1975). Bunker estimated the error in this latent heat flux at 13 percent, and the error in his solar radiation flux at 5 percent. These long-term monthly-mean heat fluxes are

shown with the heat fluxes calculated from the LOTUS data set in Figure 26. This comparison shows the ocean lost less heat to the atmosphere during 1982-83 relative to the long-term mean. This was mainly due to the smaller latent heat flux in 1982-83 than usual. Sensible heat flux was also smaller in 1982-83 than normal. Bunker's larger long-term mean sensible and latent heat fluxes are due to the greater difference in air-sea temperature and to Bunker's use of a 30 percent larger exchange coefficient in the bulk formula. Net longwave radiation in 1982-83 was comparable to the long term mean. Solar radiation in 1982-83 was normal, although about 30 W m^{-2} less radiation was received in the winter relative to the long-term mean. (Note that cloud cover was greater than usual during the winter.)

VII. CONCLUSION

The surface meteorology returned from the first year of the LOTUS experiment has been very encouraging and informative. The measurements are of high quality, and densely sampled (every few minutes) over a long period of time. For the most part, the measurements from redundant sensors agree closely; those sensors that were not so successful have been replaced on the subsequent LOTUS surface buoys.

The telemetry of meteorological data and buoy position has been extremely beneficial; not only did the telemetered data allow us to track and recover the drifting LOTUS-4 buoy, but they have sustained and encouraged our scientific excitement over the six months between deployment and recovery of the surface mooring.

With the completion of the LOTUS experiment in Spring 1984, the data set of surface meteorology should allow accurate calculation of the net heat flux to the mixed layer over an annual cycle.

ACKNOWLEDGEMENTS

We wish to thank Nancy Pennington and Rick Trask for graphics, technical, and moral support, Mary Ann Lucas for typing, and Jerry Dean and Dick Payne for answering numerous questions. Clayt Collins and Jim Valdes have also contributed essential technical input on the ARGOS project. Clayton Paulson of Oregon State Universiy provided helpful information on radiation fluxes. The LOTUS surface moorings were designed, prepared, deployed, and recovered by members of the "WHOI Buoy Group," composed of talented and energetic people from the Ocean Engineering and Physical Oceanography Departments.

LOTUS has been funded by the Office of Naval Research under contract N00014-76-C-0197, NR083-400.

References

NOTE: There are six papers in this list by A. F. Bunker, et al. Bunker (1975) is the source doument, and Bunker (1976), Bunker and Worthington (1976), and Bunker (1980) are based upon it, although the latter two include further analysis. The pair Bunker and Goldsmith (1979) and Goldsmith and Bunker (1979) describe access to the data set as it now resides at WHOI. We have used Bunker (1975, 1976) and the data set itself for our work here. The Budyko (1963) reference below is included for comparison; Bunker used it, we have not.

Anderson, R. J., and S. D. Smith, 1981. Evaporation coefficient for the sea surface from eddy flux measurements. J. Geophys. Res., 86, 449-456.

Berteaux, H. O., and N. K. Chhabra, 1973. Computer programs for the static analysis of single point moored surface and subsurface buoy systems. Woods Hole Oceano. Inst. Tech. Rept. 73-22.

Budyko, M. I., 1963. Atlas of heat balance of the world (in Russian). Glav. Geofiz. Obs., Moscow, 69 pages. See "Guide to the Atlas of the heat balance of the Earth." Translation by I. A. Donehoo. Weather Bureau, WBIT-106, Washington, D.C., 25 pages.

Bunker, A. F.., 1975. Energy exchange at the surface of the Western North Atlantic Ocean. Woods Hole Oceano. Inst. Tech. Rept. 75-3.

Bunker, A. F., 1976. Computations of surface energy flux and annual air-sea interaction cycles of the North Atlantic Ocean. Mon. Wea. Rev., 104, 1122-1140.

Bunker, 1980. Trends of variables and energy fluxes over the Atlantic Ocean from 1948 to 1972. Mon. Wea. Rev., 108, 720-732.

Bunker, A. F., and R. A. Goldsmith, 1979. Archived time-series of Atlantic Ocean meteorological variables and surface fluxes. Woods Hole Oceano. Inst. Tech. Rept. 79-3.

Bunker, A. F., and L. V. Worthington, 1976. Energy exchange charts of the North Atlantic Ocean. Bull. Amer. Meteorol. Soc., 57, 670-678.

Gill, G. C., 1976. Development and testing of a no-moving-parts static pressure inlet for use on ocean buoys. The University of Michigan. Research sponsored by NOAA Data Buoy Office, 43 pp.

Gill, G. C., 1979. Development of a small rugged radiation shield for air temperature measurement on drifting buoys. The University of Michigan. Research sponsored by NOAA Data Buoy Office, 23 pages.

Goldsmith, R. A., and A. F. Bunker, 1979. Woods Hole Oceanographic Institution collection of Climatology and Air/Sea Interaction (CASI) data. Woods Hole Oceano. Inst. Tech. Rept. 79-70.

Large, W. G., and S. Pond, 1982. Sensible and latent heat flux measurements over the ocean. J. Phys. Oceanogr., 12, 464-482.

List, R. J., 1951. Smithsonian Meteorological Tables, Smithsonian Institution, Washington, D. C., 527 pp.

Payne, R. E., 1974. A buoy-mounted meteorological recording package. Woods Hole Oceano. Inst. Tech. Rept. 74-40.

Payne, R. E., 1981. Performance characteristics of some wind sensors. Woods Hole Oceano. Inst. Tech. Rept. 81-101.

Reed, R. K., 1975. An evaluation of formulas for estimating clear-sky insolation over the ocean. NOAA Technical Report, ERL 352-PMEL 26, 25 pages.

Reed, R. K., 1977. On estimating insolation over the ocean. J. Phys. Oceanogr., 7, 482-485.

Seckel, G. R., and F. H. Beaudry, 1973. The radiation from sun and sky over the North Pacific Ocean (abstract). Trans. Amer. Geophys. Un., 54, 1114.

Simpson, J. J., and C. A. Paulson, 1979. Mid-ocean observations of atmospheric radiation. Quart. J. Roy. Meteorol. Soc., 105, 487-502.

Stevenson, J. W., 1982. Computation of heat and momentum fluxes at the sea surface during the Hawaii to Tahiti Shuttle experiment. Joint Institute for Marine and Atmospheric Research, University of Hawaii, 82-0044, HIG-82-4.

Sverdrup, H. V., M. W. Johnson, R. H. Fleming, 1942. The Oceans, Their Physics, Chemistry, and General Biology, Prentice Hall.

Tabata, S., 1964. Insolation in relation to cloud amount and sun's altitude. In: Studies on Oceanography, edited by K. Yoshida, University of Tokyo, Tokyo, 202-210.

Tabata, S., 1973. A simple but accurate formula for the saturation vapor pressure over liquid water. J. Appl. Meteorol., 12, 1410-1411.

Trask, R. P., M. G. Briscoe, and N. J. Pennington, 1982. Long Term Upper Ocean Study (LOTUS): A summary of the historical data and engineering test data. Woods Hole Oceano. Inst. Tech. Rept. 82-53.

APPENDIX

Bulk formulas are used to estimate heat fluxes (net longwave radiative, latent, and sensible) at the sea surface.

The net heat flux at the sea surface is:

$$A = Q_S (1 - \alpha) - IR - S_E - L_E$$

where Q_S is the shortwave solar radiation

α is the albedo

IR is the net longwave radiation

L_E is the latent heat flux

S_E is the sensible heat flux

We have tried to be consistent with Bunker (1975) in our heat flux notation.

The bulk formulas are empirical and there are many to choose from in the literature. Recent work by Large and Pond (1982) and Stevenson (1982) as well as Bunker (1975) have suggested the heat flux parameterizations used in this report. The formulas assume all meteorological measurements have been made at a height of 10 m. Corrections for height and stability have not been applied since the water vapor (hence atmospheric stability) data were lacking. These corrections could amount to 10 percent in wind speed and air temperature measured at the LOTUS site (Payne, personal communication).

Net Longwave Radiation

The empirical formula for the net longwave radiation under clear skies is:

$$IR_o = 0.97 \sigma T_s^4 (0.39 - 0.05 e_a^{1/2}) +$$

$$4(.97) \sigma T_s^3 (T_s - T_a)$$

where .97 is the emissivity at the sea surface, $\sigma = 5.673 \times 10^{-8}$ W m^{-2} K^4 is the Stefan-Boltzmann constant, e_a is the water vapor pressure in mb, T_s and T_a are the water and air temperature in degrees Kelvin, respectively. This formula comes from Stevenson (1982). The cloud correction factor

$$IR/IR_o = (1 - 0.8N)$$

where N is cloudiness in tenths, has been used by Simpson and Paulson (1979) for their data collected at 35°N, 155°W on FLIP.

Since LOTUS-3 did not provide measurements of water vapor, the term e_a in the longwave radiative flux equation was estimated using historical data from Bunker (1975). We have used e_a = 25 mb throughout. Fortunately, the longwave flux is the smallest of the terms in the heat budget equation.

Cloud Cover

The method for deriving cloud cover, N, (since direct observations of cloud cover were not available) is discussed below.

Daylight-averaged cloud cover was inferred from direct measurements of solar radiation. The reduction of insolation by clouds can be expressed as:

$$Q_S/Q_o = 1 - 0.716C + 0.00252\alpha$$

according to Tabata (1964), where

C is the fraction in tenths of the sky that is covered by clouds

α is the noon altitude of the sun in degrees calculated from

$$\sin(2\pi\alpha/360) = \cos(\ell - (2\pi/360)(23.87\sin(2\pi(t-82)/365)))$$

where ℓ is the latitude in radians,

t is the time of year in days,

Q_o is the daily averaged short wave radiation under clear skies, calculated from the following empirical formula given by Seckel and Beaudry (1973):

$$Q_o = A_0 + A_1 \cos\phi + B_1 \sin\phi + A_2 \cos 2\phi + B_2 \sin 2\phi$$

$$A_0 = -15.82 + 326.87 \cos\ell$$

$$A_1 = 9.63 + 192.44 \cos(\ell + \pi/2)$$

$$B_1 = -3.27 + 108.70 \sin\ell$$

$$A_2 = -0.64 + 7.80 \sin 2(\ell - \pi/4)$$

$$B_2 = -0.50 + 14.42 \cos 2(\ell - \pi/36)$$

The units of Q_o are in W m^{-2}, $\phi = (t-21)2\pi/365$.

Insolation calculated from Tabata (1964) is accurate to approximately 20 W m^{-2} (Reed, 1977). Figure 27 shows the calculated curve of insolation under clear skies, the measured insolation plus 60 W m^{-2}, and the derived cloud amounts. Reed's (1977) cloud correction formula gave larger cloud amounts (4 - 18 tenths) than Tabata's (1964) formula.

Sensible Heat Flux

The empirical formula for the sensible heat flux is

$$S_E = \rho_a C_{pa} C_H (T_s - T_a) U_{10}$$

where $\rho_a = 1178$ g m^{-3} is the air density,

$C_{pa} = 1.005$ W $s(g°C)^{-1}$ is the heat capacity for dry air,

C_H is the transfer coefficient for sensible heat,

T_s is the water temperature (°C),

T_a is the air temperature (°C), and

U_{10} is the wind speed (m s^{-1}).

This formula is used by Bunker (1975). Stevenson (1982) includes an additional term which depends on the moisture content of the air.

C_H is difficult to specify accurately without an estimate of the stability of the air. Since stability depends on the water vapor content of the air, we cannot make a direct estimate of C_H. Anderson and Smith (1981) find C_H to be

$$C_H = \begin{cases} 0.82 \times 10^{-3} & \text{stable} \\ 1.12 \times 10^{-3} & \text{unstable} \end{cases}$$

We take $C_H = 1 \times 10^{-3} \pm .2 \times 10^{-3}$ as a first estimate.

Latent Heat Flux

The empirical formula for the latent heat flux at the sea surface is

$$L_E = \rho_a C_E E (q_s - q_a) U_{10}$$

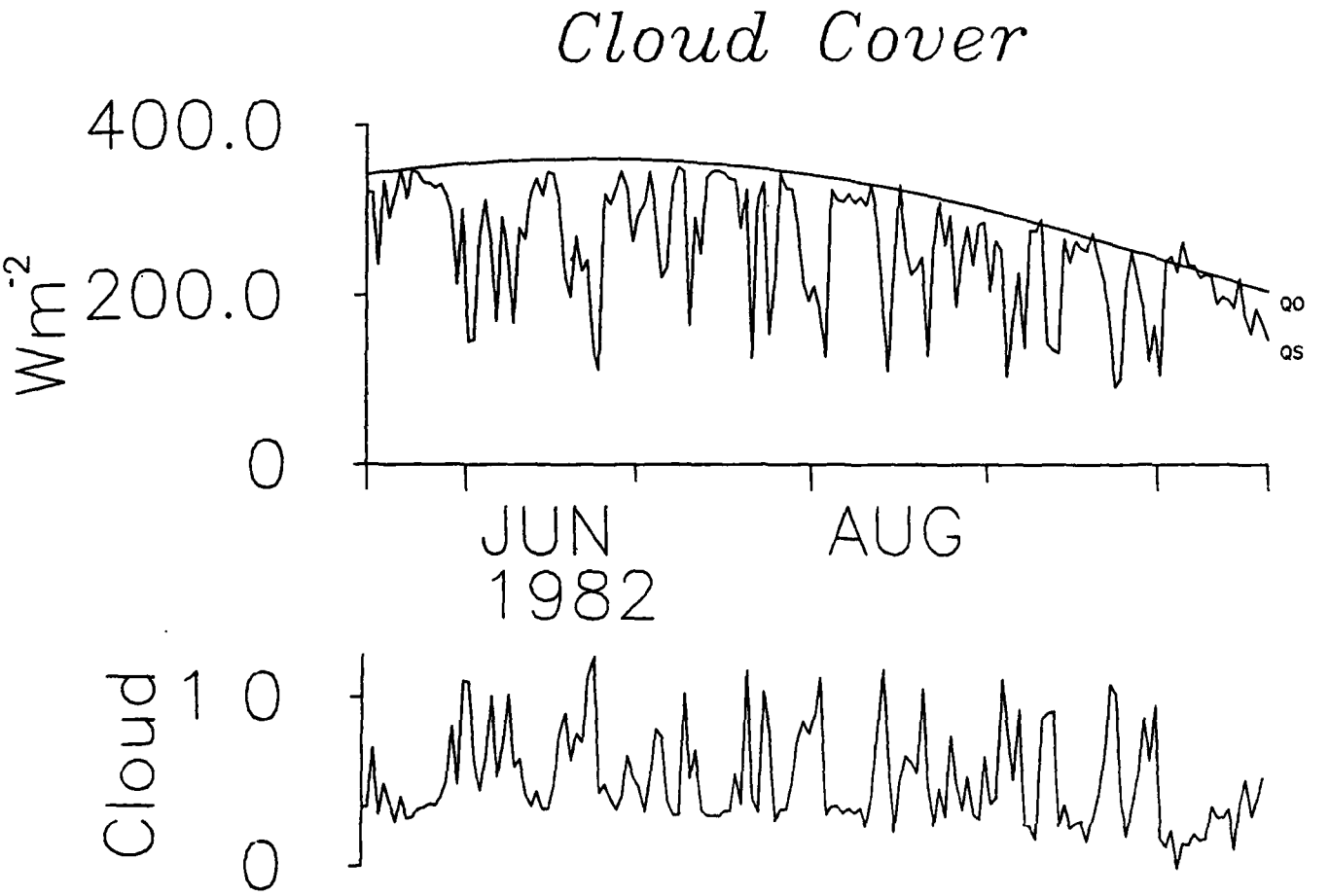

Figure 27. (a) Measured insolation (QS) augmented by 60 W m^{-2}, and clear-sky insolation (QO) in W m^{-2}. (b) Derived daily-averaged cloud cover in tenths, from LOTUS-3.

where

C_E = evaporation coefficient (1.3×10^{-3}),

E = latent heat of evaporation (2441 W s g^{-1}),

q_s = saturation specific humidity at sea surface temperature, and

q_a = specific humidity of the air.

The saturation specific humidity at the sea surface temperature, q_s, was computed as follows (most of the definitions come from the Smithsonian Meteorological Tables (List, 1951)): a simplified expression for the saturation vapor pressure over pure water is given by (Tabata, 1973):

$$\log_{10} e_w = 8.42926609 - 1.82717483 \left(\frac{1000}{T_{wk}}\right) - 0.071208271 \left(\frac{1000}{T_{wk}}\right)^2$$

where e_w is in millibars, and T_{wk} is the sea surface temperature in degrees Kelvin. Saturation vapor pressure is slightly different over salt water than over pure water. The dependence is (Sverdrup, Johnson, and Fleming, 1942)

$$e_s = e_w(1 - 0.000537S)$$

where e_s is the saturation vapor pressure over salt water, and S is the salinity in °/₀₀. At S=35°/₀₀, e_s is 2 percent less than e_w. $e_s = 0.98\ e_w$ has been assumed throughout.

Next, the saturation mixing ratio (w_w) over salt water was computed from the definition

$$W_w = \frac{\varepsilon f e_s}{p - f e_s}$$

where

ε = 0.6219,

p = barometric pressure in millibars,

e_s = saturation vapor pressure, and

f is the correction factor for the departure of the mixture of air and water vapor from ideal gas laws, and can be approximated by

$f = 1.004 \pm .001$.

Finally, the saturation specific humidity was computed from the saturation mixing ratio by

$$q_s = \frac{w_w}{1 + w_w} .$$

q_a, the specific humidity of the air, was computed from relative humidity using the following algorithm:

by definition,

$$r = \frac{w}{w_w} \times 100$$

where r = relative humidity in percent,

w = mixing ratio, and

w_w = saturation mixing ratio.

So $w = \frac{r}{100} w_w$

where w_w is found above.

By definition, $q_a = \frac{w}{1 + w}$.

Because LOTUS-3 did not provide direct measurements of water vapor content in the air, we have resorted to the Bowen ratio for estimating the latent heat flux:

$$L_E = S_E/B$$

where B is the Bowen ratio.

This procedure has been questioned but the following analysis shows the monthly-averaged fluxes of latent heat may be usefully determined from the Bowen ratio.

Monthly values of the Bowen ratio have been determined from monthly-mean sensible and latent heat fluxes computed by Bunker from historical data at the LOTUS site (Bunker, 1975). The following values represent a 13-year average (1960-1972) of the Bowen ratio and standard deviation (s) for each month:

	May	June	July	Aug	Sept	Oct	Nov	Dec	Jan	Feb	Mar	Apr
B	.10	.08	.07	.08	.11	.14	.19	.25	.29	.29	.25	.17
s	.033	.018	.019	.014	.014	.020	.021	.027	.107	.102	.036	.030
s/B	.33	.23	.27	.18	.13	.14	.11	.11	.37	.35	.14	.18

MANDATORY DISTRIBUTION LIST

FOR UNCLASSIFIED TECHNICAL REPORTS, REPRINTS, AND FINAL REPORTS PUBLISHED BY OCEANOGRAPHIC CONTRACTORS OF THE OCEAN SCIENCE AND TECHNOLOGY DIVISION OF THE OFFICE OF NAVAL RESEARCH

(REVISED JUNE 1983)

1 *Deputy Under Secretary of Defense*
(Research and Advanced Technology)
Military Assistant for Environmental Science
Room 3D129
Washington, DC 20301

Office of Naval Research
800 North Quincy Street
Arlington, Va 22217
3 *ATTN: Code 483*
1 *ATTN: Code 420C*
2 *ATTN: 102B*

Commanding Officer
Naval Research Laboratory
Washington, DC 20375
6 *ATTN: Library Code 2627*
1 *ATTN: Library Code 2620, Mr. Peter Imhof*

12 *Defense Technical Information Center*
Cameron Station
Alexandria, VA 22314
ATTN: DCA

Commander
Naval Oceanographic Office
NSTL Station
Bay St. Louis, MS 39522
1 *ATTN: Code 8100*
1 *ATTN: Code 6000*
1 *ATTN: Code 3300*

1 *NODC/NOAA*
Code D781
Wisconsin Avenue, N.W.
Washington, DC 20235

* See also the NOTE at the beginning of the References.